Published April 28, 2014

Local control of TRPV4 channels by AKAP150-targeted PKC in arterial smooth muscle

Jose Mercado,[1] Rachael Baylie,[3] Manuel F. Navedo,[4] Can Yuan,[1] John D. Scott,[2] Mark T. Nelson,[3] Joseph E. Brayden,[3] and Luis F. Santana[1]

[1]Department of Physiology & Biophysics and [2]Howard Hughes Medical Institute, Department of Pharmacology, University of Washington, Seattle, WA 98195
[3]Department of Pharmacology, University of Vermont, Burlington, VT 05405
[4]Department of Pharmacology, University of California, Davis, Davis, CA 95616

Transient receptor potential vanilloid 4 (TRPV4) channels are Ca^{2+}-permeable, nonselective cation channels expressed in multiple tissues, including smooth muscle. Although TRPV4 channels play a key role in regulating vascular tone, the mechanisms controlling Ca^{2+} influx through these channels in arterial myocytes are poorly understood. Here, we tested the hypothesis that in arterial myocytes the anchoring protein AKAP150 and protein kinase C (PKC) play a critical role in the regulation of TRPV4 channels during angiotensin II (AngII) signaling. Super-resolution imaging revealed that TRPV4 channels are gathered into puncta of variable sizes along the sarcolemma of arterial myocytes. Recordings of Ca^{2+} entry via single TRPV4 channels ("TRPV4 sparklets") suggested that basal TRPV4 sparklet activity was low. However, Ca^{2+} entry during elementary TRPV4 sparklets was ~100-fold greater than that during L-type $Ca_V1.2$ channel sparklets. Application of the TRPV4 channel agonist GSK1016790A or the vasoconstrictor AngII increased the activity of TRPV4 sparklets in specific regions of the cells. PKC and AKAP150 were required for AngII-induced increases in TRPV4 sparklet activity. AKAP150 and TRPV4 channel interactions were dynamic; activation of AngII signaling increased the proximity of AKAP150 and TRPV4 puncta in arterial myocytes. Furthermore, local stimulation of diacylglycerol and PKC signaling by laser activation of a light-sensitive G_q-coupled receptor (opto-α_1AR) resulted in TRPV4-mediated Ca^{2+} influx. We propose that AKAP150, PKC, and TRPV4 channels form dynamic subcellular signaling domains that control Ca^{2+} influx into arterial myocytes.

INTRODUCTION

Arterial myocytes have the intrinsic ability to contract in response to increases in intravascular pressure (Bayliss, 1902). It has been proposed that this myogenic response is initiated by the stretch-induced activation of the nonselective cation channels TRPP2, TRPC6, and TRPM4, which depolarize arterial myocytes (Welsh et al., 2002; Earley et al., 2004; Spassova et al., 2006; Narayanan et al., 2013). Membrane depolarization activates voltage-gated L-type $Ca_V1.2$ channels (Harder et al., 1987; Fleischmann et al., 1994; Rubart et al., 1996; Jaggar et al., 1998). The influx of Ca^{2+} via a single $Ca_V1.2$ channel can be optically detected in the form of a "$Ca_V1.2$ sparklet" (Navedo et al., 2005; Amberg et al., 2007). Simultaneous activation of multiple $Ca_V1.2$ sparklets induces a cell-wide increase in intracellular Ca^{2+} ($[Ca^{2+}]_i$) that activates myosin light chain kinase and thus triggers contraction. This myogenic response is critical for the process of autoregulation of blood flow.

Cerebral artery myocytes express transient receptor potential vanilloid 4 (TRPV4) channels. Like $Ca_V1.2$ channels, TRPV4 channels are highly permeable to Ca^{2+} (Liedtke et al., 2000; Strotmann et al., 2000). However, while $Ca_V1.2$ channels are critical for contraction, TRPV4 channels have been linked to relaxation (Earley et al., 2005, 2009). According to this model, the endothelium-derived factor 11,12-epoxyeicosatrienoic acid (11,12-EET) activates TRPV4 channels, and the resulting influx of Ca^{2+} activates nearby ryanodine receptors (RyRs), which release Ca^{2+} from the sarcoplasmic reticulum in the form of a Ca^{2+} spark. Local Ca^{2+} sparks activate large-conductance, Ca^{2+}-activated K^+ (BK) channels. This hyperpolarizes the membrane and closes $Ca_V1.2$ channels, thereby decreasing $[Ca^{2+}]_i$ and causing myocyte relaxation. One implication of this model is that the strength of the TRPV4-induced arterial myocyte hyperpolarization depends on the magnitude, frequency, and location of

Correspondence to Luis F. Santana: santana@u.washington.edu; or Joseph E. Brayden: joe.brayden@uvm.edu

Abbreviations used in this paper: 11,12-EET, 11,12-epoxyeicosatrienoic acid; AngII, angiotensin II; ccRICS, cross-correlation raster image correlation spectroscopy; DAG, diacylglycerol; EGFP, enhanced green fluorescent protein; GSD, ground state depletion; RICS, raster image correlation spectroscopy; ROI, region of interest; RyR, ryanodine receptor; TIRF, total internal reflection fluorescence; tRFP, tag red fluorescent protein; WT, wild type.

© 2014 Mercado et al. This article is distributed under the terms of an Attribution–Noncommercial–Share Alike–No Mirror Sites license for the first six months after the publication date (see http://www.rupress.org/terms). After six months it is available under a Creative Commons License (Attribution–Noncommercial–Share Alike 3.0 Unported license, as described at http://creativecommons.org/licenses/by-nc-sa/3.0/).

The Rockefeller University Press $30.00
J. Gen. Physiol. Vol. 143 No. 5 559–575
www.jgp.org/cgi/doi/10.1085/jgp.201311050

Supplemental Material can be found at:
http://jgp.rupress.org/content/suppl/2014/04/22/jgp.201311050.DC1.html

The Journal of General Physiology

Downloaded from jgp.rupress.org on June 23, 2014

Published April 28, 2014

the Ca^{2+} signals produced by TRPV4 channels. These relationships, as well as the molecular mechanisms regulating local TRPV4 Ca^{2+} signals in arterial myocytes, have not been clearly established.

PKC is an important signaling molecule in the regulation of TRPV4 channels (Cao et al., 2009; Fan et al., 2009). In arterial myocytes, PKC is activated by an increase in local $[Ca^{2+}]_i$ and diacylglycerol (DAG) produced by the activation of G_q protein–coupled receptors, including angiotensin II (AngII) receptors. PKC is targeted to the sarcolemma of arterial myocytes by the anchoring protein AKAP150 (Navedo et al., 2008). Biochemical and cell-based studies suggest a potential mechanism for local Ca^{2+}-dependent activation of PKC (Hoshi et al., 2010). The model suggests that as Ca^{2+} enters the cell, it recruits Ca^{2+}/calmodulin to AKAP150, which then releases PKC from the AKAP150 complex, allowing it to phosphorylate nearby targets rapidly. At present, a role for AKAP150-anchored PKC in the modulation of arterial myocyte TRPV4 channels is unclear.

In this study, we combined electrophysiological and a variety of microscopy approaches to investigate the spatial organization and function of TRPV4 channels in arterial myocytes. Super-resolution imaging and cross-correlation raster image correlation spectroscopy (ccRICS) revealed new insights on how individual AKAP150 and TRPV4 channel complexes are organized in the cell membrane. We recorded subcellular Ca^{2+} signals resulting from the opening of single TRPV4 channels ("TRPV4 sparklets"). Activation of AngII signaling increased TRPV4 sparklet activity, and this activity was dependent on AKAP150 and PKC. We propose a mechanistic model in which TRPV4 channels dynamically interact with AKAP150, thereby targeting PKC to these channels. This creates local signaling domains that control TRPV4 Ca^{2+} influx into arterial myocytes.

MATERIALS AND METHODS

Arterial diameter measurements and isolation of arterial myocytes

Rats (Sprague-Dawley) as well as wild type (WT), AKAP150-null ($AKAP150^{-/-}$), and TRPV4-null ($TRPV4^{-/-}$) mice (C57BL/6J) were used in this study. Animals were euthanized with a lethal dose of sodium pentobarbital (250 mg/kg IP), as approved by the University of Washington (rats, WT mice, and $AKAP150^{-/-}$ mice) or University of Vermont (WT and $TRPV4^{-/-}$ mice) Institutional Animal Care and Use Committees. For diameter measurements, cerebral arteries were dissected, cleaned, and transferred to an arteriograph chamber, where they were cannulated with a glass micropipette. The endothelium was removed by passage of an air bubble through the lumen of the artery. The proximal pipette was attached to a servo-controlled pressure-regulating device (Living Systems Instrumentation). Arteries were pressurized (60 mmHg) for >45 min in a saline solution (36°C) containing (in mM) 119 NaCl, 4.7 KCl, 1.2 KH_2PO_4, 1.2 $MgCl_2$, 2 $CaCl_2$, 10 glucose, and 25 $NaHCO_3$, pH 7.4. This solution was aerated with a normoxic gas mixture (21% O_2, 5% CO_2, balance N_2). Inner diameter was monitored using video microscopy and edge-detection software (Ionoptix). Loss of the endothelium was confirmed by the lack of dilatory response to the endothelium-dependent vasodilator NS309 (1 µM). Maximum contractile responses were induced by exposing the arteries to a saline solution with 100 nM of the thromboxane analogue U46619. Myocytes for total internal reflection fluorescence (TIRF), confocal, and super-resolution microscopy were dissociated from cerebral arteries using previously described approaches (Amberg and Santana, 2003).

Culture and transfection of tsA-201 cells

We kept tsA-201 cells in Dulbecco's modified Eagle medium supplemented with 10% fetal bovine serum and a 1% penicillin/streptomycin antibiotic solution. Cells were transiently transfected using jetPEI and plated onto 25-mm coverslips (0.13–0.17-mm thick). The plasmids used in this study encoded the enhanced green fluorescent protein (EGFP), tag red fluorescent protein (tRFP), mouse TRPV4 fused to EGFP or mCherry, AKAP150 fused to EGFP, AKAP79 fused to mCherry, PKCα, the transcription factor CIBN fused to EGFP and a CAAX box (CIBN-EGFP-CAAX), and opto-α_1 adrenergic receptors (opto-α_1AR) fused to YFP. TRPV4, CIBN-EGFP-CAAX, and opto-α_1AR-YFP were provided by S. Philipp (Saarland University, Saarbrücken, Germany), P. De Camilli (Yale University, New Haven, CT), and K. Deisseroth (Stanford University, Stanford, CA), respectively. We fused TRPV4 channels to mCherry (TRPV4-mCherry) or EFGP (TRPV4-EGFP) at their carboxy tail. Successfully transfected cells were identified on the basis of EGFP, YFP, tRFP, or mCherry fluorescence. Experiments were performed 24–48 h after transfection. Plasmids encoding EGFP and tRFP were purchased from Invitrogen and Evrogen, respectively.

Confocal immunofluorescence microscopy

Arterial myocytes were fixed, permeabilized, and exposed to anti-TRPV4 (H-79) and anti-AKAP150 (N-19) antibodies (Santa Cruz Biotechnology, Inc.). Alexa Fluor 488–conjugated donkey anti–goat (5 µg/ml) and an Alexa Fluor 568–conjugated donkey anti–rabbit (5 µg/ml; Molecular Probes) were used as secondary antibodies. Confocal images were acquired with a confocal microscope (Fluoview FV1000; Olympus) equipped with a UPlanS-Apochromat 60× (NA 1.2) water immersion objective lens. The resolution of our confocal microscope was ∼250 nm in the x-y axis and ∼800 nm in the z axis. Myocytes were imaged with a zoom of 3.5 (1,024 × 1,024 pixel images; pixel size = 0.1 µm). Alexa Fluor 488 and Alexa Fluor 568 were excited using 473 nm and 559 nm lasers, respectively. Fluorescence was quantified by measuring the intensity of pixels above a threshold defined as the mean nonspecific fluorescence intensity within cells (i.e., cell background, secondary antibody only) plus three times its SD. We calculated the Pearson's coefficient of TRPV4 and AKAP150 images to quantify the degree of overlap between fluorophores within the confocal volume.

Super-resolution microscopy

We used a ground state depletion (GSD) system (Leica) to generate TIRF and super-resolution localization images of TRPV4 and AKAP150 in arterial myocytes. The system is coupled to an inverted microscope (DMI6000B; Leica). Images were obtained using 100× (NA 1.47) or 160× HCX Plan-Apochromat (NA 1.47) oil immersion lenses and an electron microscopy charge-coupled device (EMCCD) camera (iXon3 897; Andor Technology). Cells were fixed, permeabilized, and exposed to antibodies targeting TRPV4 and AKAP150 as described in the immunofluorescence section above. We used secondary antibodies conjugated to Alexa Fluor 488 (TRPV4) or Alexa Fluor 647 (AKAP150). During imaging, cells were kept in PBS (pH 7.4) containing 30 mM mercaptoethylamine (MEA). Fluorophores were excited with 300 mW 488 and 647 nm

Downloaded from jgp.rupress.org on June 23, 2014

Published April 28, 2014

lasers. The power of the light exiting the lens was ∼3–5% of the total power of these lasers.

The localization of fluorescence particles was determined by fitting single molecule fluorescence signals with a 2D Gaussian function using LASAF software (Leica). The localization accuracy (i.e., standard error) of the system is limited by the statistical noise of photon counting (Heisenberg, 1930; Fölling et al., 2008; Schermelleh et al., 2010). Thus, assuming the point-spread functions are Gaussian, the precision of localization is proportional to DLR/√N, where DLR is the diffraction-limited resolution of a fluorophore and N is the number of detected photons. Accordingly, we estimated a lateral localization accuracy of ∼13 nm for Alexa Fluor 488 and ∼11 nm for Alexa Fluor 647. The effective resolution (i.e., width at half-maximum amplitude) of our system was ∼30 nm and ∼26 nm for Alexa Fluor 488– and Alexa Fluor 647–associated fluorescence. Images were rendered to a pixel size of 5 or 10 nm. For analysis, we set an event threshold of 60 events per pixel. High-resolution localization images were reconstructed using the coordinates of centroids obtained from these fluorescent particles from >20,000 images. The number of events detected in cells exposed to primary and secondary antibodies ranged between 220,000 and 800,000. Only 3,000–4,290 events were detected in cells exposed to secondary antibodies only.

We used an object-based analysis to measure the distance between AKAP150 and TRPV4 channels in super-resolution localization images using National Institutes of Health ImageJ software with the JACoP colocalization analysis plug-in. This analysis uses image segmentation by connexity analysis (Lachmanovich et al., 2003; Bolte and Cordelières, 2006). In brief, this process involves the systematic inspection of the neighborhood (8 pixels in 2D) of a pixel (reference pixel). All adjacent pixels with intensities above a set threshold limit are considered to be part of the same structure as the reference pixel and represent individualized particles (individualized structures). After segmentation, centroids are determined from each particle/structure. Centroids are the geometrical centers of the particle including the global shape of the particle/structure. We measured the distance between centroids in the green and red channel. Control experiments examined the distance of Alexa Fluor 488– and Alexa Fluor 647–conjugated secondary antibodies.

Patch-clamp electrophysiology

We controlled membrane potential and recorded membrane currents from arterial myocytes and tsA-201 cell using an Axopatch 200B amplifier. During experiments, cells were continuously superfused with a solution containing 142 mM NaCl, 6 mM KCl, 1 mM $MgCl_2$, 10 mM HEPES, 10 mM glucose, and 2 mM $CaCl_2$ adjusted to pH 7.4. Pipettes were filled with a solution composed of 100 mM Na^+-glutamate, 20 mM NaCl, 1 mM $MgCl_2$, 10 mM EGTA, 10 mM HEPES, 4 mM Na_2-ATP, and 42 mM mannitol, pH 7.2. To determine the TRPV4 current–voltage relationship, cells expressing TRPV4 channels were voltage-clamped to −70 mV. Whole-cell TRPV4 currents were recorded while cells were submitted to a 1-s voltage ramp from −100 to +120 mV. Electrophysiological signals were acquired at a frequency of 5–10 kHz and low-pass filtered at 1 kHz. A voltage error of 12 mV resulting from the liquid junction potential of these solutions was corrected offline. All patch-clamp experiments were performed at room temperature (22–25°C). Currents were analyzed using pClamp 9.0 software (Axon Instruments).

$[Ca^{2+}]_i$ imaging

TRPV4 and $Ca_V1.2$ sparklets were recorded in voltage-clamped (membrane potential = −70 mV) arterial myocytes and tsA-201 cells. We used a through-lens TIRF microscope built around an inverted microscope (IX-70; Olympus) equipped with a Plan-Apochromat (60×; NA 1.49) oil immersion lens (Olympus) and an EMCCD camera (iXON; Andor Technology). To monitor $[Ca^{2+}]_i$, 200 µM of the Ca^{2+} indicator Fluo-5F was added to the pipette solution described earlier. Rhod-2 (200 µM) was used in experiments in which EGFP-tagged proteins were expressed. Excitation of Fluo-5F and Rhod-2 was achieved with 491- or 563-nm lasers, respectively. The inclusion of a relatively fast Ca^{2+} indicator and the much slower Ca^{2+} buffer EGTA (10 mM) restricted Ca^{2+} signals to the vicinity of the point of Ca^{2+} influx (Zenisek et al., 2003). Accordingly, the radius of TRPV4 sparklets was 0.50 ± 0.03 µm.

TIRF images were acquired at a frequency of 100–300 Hz using TILL Image software. Sparklets were detected and analyzed using custom software written in MATLAB (Navedo et al., 2010). Fluorescence intensity values were converted to nanomolar units as described previously (Navedo et al., 2005, 2006). All-points or event amplitude histograms were generated from $[Ca^{2+}]_i$ records. Histograms were fit with the following multicomponent Gaussian function:

$$N = \sum_{j=1}^{n} a_j \times exp\left[-\frac{\left(\Delta\left[Ca^{2+}\right]i - jq\right)^2}{2jb} \right],$$

where a and b are constants, and $\Delta[Ca^{2+}]_i$ and q are the change in intracellular Ca^{2+} concentration and the quantal unit of Ca^{2+} influx, respectively. We determined the activity of sparklets by calculating the nP_s of each sparklet size, where n is the quantal level number and P_s is the probability that a quantal sparklet event is active. In addition, the signal mass of sparklets was determined. Details of the nP_s and signal mass analyses can be found elsewhere (ZhuGe et al., 2000; Zou et al., 2002; Navedo et al., 2005, 2006). To calculate the Ca^{2+} flux associated with the opening of a TRPV4 channel, TRPV4 sparklets and currents were simultaneously recorded. From these records, the Ca^{2+} signal mass of a TRPV4 sparklet and the charge (in coulombs) of the underlying TRPV4 current (Q_{TRPV4}) were calculated. Q_{TRPV4} was determined by integrating TRPV4 currents.

Light-induced activation of opto-α_1AR

We used a confocal microscope to activate opto-α_1AR and monitor $[Ca^{2+}]_i$ in voltage-clamped tsA-201. To avoid unintended activation of opto-α_1AR by ambient light, tsA-201 cells expressing this protein were kept in the dark or under red light. For $[Ca^{2+}]_i$ imaging experiments, cells were loaded with the Ca^{2+} indicator Rhod-2 (200 µM) via the patch pipette. Rhod-2 was excited with 559 nm light. Xestospongin C (3 µM) was also added to the patch pipette solution used in these experiment to block Ca^{2+} release via IP_3 receptors (IP_3Rs). Confocal images were acquired every 500 ms. Local activation of opto-α_1AR during these experiments was achieved by illuminating a small portion (3–12 μm^2) of the surface membrane for 1 min with 473 nm light. $[Ca^{2+}]_i$ images were captured before, during, and after photo-activation of opto-α_1AR. Whole-cell TRPV4 currents were recorded before and after cell-wide activation of opto-α_1AR.

FRAP

We used FRAP to estimate the mobility of AKAP150-EGFP or TRPV4-EGFP expressed in the surface membrane of tsA-201 cells. We imaged tsA-201 cells expressing one of these proteins with our confocal microscope. The imaging protocol involved the acquisition of 10 control 512 × 512 pixel images (i.e., prebleaching) at a frequency of 1 Hz. This was followed by high-intensity illumination of a region of interest (ROI) with an area of ∼3–12 μm^2 with 473 nm light (10 µW) for 10–20 s to photobleach AKAP150-EGFP or TRPV4-EGFP. The ROIs comprised ∼0.3–1% of the cell membrane. Images were continuously recorded during the photobleaching step until the fluorescence intensity in the bleached

Downloaded from jgp.rupress.org on June 23, 2014

Published April 28, 2014

ROI reached steady state. During analysis, we determined the time course of the spatially averaged, background-subtracted fluorescence intensity in the ROI. Fluorescence intensity values were normalized to prebleaching levels. The mobile fraction (f_m) was calculated by dividing the steady-state fluorescence intensity after photobleaching by the fluorescence intensity under control conditions. The immobile fraction (f_i) was equal to $1 - f_m$.

Raster image correlation spectroscopy (RICS) and ccRICS

We performed RICS and ccRICS analyses to determine the diffusion coefficients and interactions between TRPV4-mCherry and AKAP150-EGFP in living tsA-201 cells. Because the mathematical basis and experimental implementation of these techniques have been described in great detail in a series of papers by E. Gratton and colleagues (Digman et al., 2009a,b; Rossow et al., 2010), we will describe them here briefly. Images were acquired with our confocal microscope (FV1000), running in pseudo-photon counting mode. A 60× water immersion objective lens (NA 1.2) was used. Pixel size and dwell time were 50 nm and 12.5 µs, respectively. Files contained 100 images (256 × 256 pixels). RICS and ccRICS analyses were performed using SimFCS software as described previously (Digman et al., 2009a,b; Rossow et al., 2010; Dixon et al., 2012). Images were collected from the top and middle sections of the cells.

Because TRPV4-mCherry and AKAP150-EGFP fluorescence showed similar diffusion rates regardless of whether images were taken from the top or middle of the cell, ccRICS analysis was performed using images from the center of the cell. The analysis involves subtraction of background, elimination of slow or immobile proteins, and image correlation. To do this, we performed a moving average background subtraction (referred to here as moving average or MAV), which involves first calculating the average of a range of consecutive images then subtracting it from the image in the middle of this range. Because the diffusion coefficient of membrane-associated proteins tends to be slow, we used an MAV of 60 frames, which, given our imaging settings, emphasizes slower fluorescence intensity fluctuations lasting up to 69 s. The detection of protein–protein interactions using ccRICS assumes that fluorescent proteins do not undergo fluorescence resonance energy transfer (FRET) and that bleed-through between the two detection channels is <5% (Digman et al., 2009a; Rossow et al., 2010). Accordingly, we did not detect FRET (donor dequenching method) between our AKAP150-EGFP and TRPV4-mCherry constructs. Moreover, bleed-through of EGFP into the mCherry channel and vice versa was 4.2% and 1.1%, respectively.

Quantitative real-time polymerase chain reaction (qPCR)

Total RNA was isolated from ∼60 arterial myocytes or segments from WT or AKAP150$^{-/-}$ using the RNAeasy Micro kit (QIAGEN) according to the manufacturer's instructions. cDNA was synthesized from 1 µg of total RNA using the SuperScript III kit (Invitrogen). qPCR was performed on an ABI Prism 7000 Sequence Detection System using the QuantiTect SYBR Green PCR kit (QIAGEN). Samples were amplified with the following protocol: 45 cycles of 94°C for 15 s; 56°C for 30 s; 72°C for 30 s. β-Actin transcript levels were used to normalize expression of TRPV4. Primers for TRPV4 (Mm_TRPV4_1_SG) and β-actin (Mm_Actb_2_SG) were obtained from QIAGEN. Real-time PCR data were analyzed using the ΔΔCT method.

Chemicals and statistics

AngII, 11,12-EET, GSK1016790A, buffers, and salts were purchased from Sigma-Aldrich. The PKC inhibitor Gö6976 was purchased from EMD Millipore. Fluorescent Ca^{2+} indicators, cell culture media, and supplements were bought from Life Technologies. The jetPEI transfection reagent was purchased from Polyplus. Data with a normal distribution are presented as mean ± SEM. Two sample comparisons of parametric data were performed using a Student's *t* test. A Mann-Whitney test was used for nonparametric data. A p-value of <0.05 was considered significant.

Online supplemental material

Fig. S1 shows data suggesting that TRPV4 sparklet duration is increased during GSK and AngII exposure to arterial myocytes. Fig. S2 shows the effects of AngII on $Ca_V1.2$ and TRPV4 sparklets in arterial myocytes. Fig. S3 shows super-resolution localization maps of arterial myocytes labeled with TRPV4- and AKAP150-specific antibodies in the absence or presence of AngII. Online supplemental material is available at http://www.jgp.org/cgi/content/full/jgp.201311050/DC1.

RESULTS

Super-resolution imaging reveals that TRPV4 channels form puncta of varied sizes in arterial myocytes.

A combination of confocal, TIRF, and super-resolution GSD microscopy was used to investigate the spatial organization of TRPV4 channels in arterial myocytes. The lateral resolution of our confocal microscope was ∼250 nm. Fig. 1 A shows a confocal image of a representative fixed arterial myocyte labeled with a TRPV4-specific antibody. TRPV4-associated fluorescence was observed all along the sarcolemma.

TIRF and super-resolution GSD microscopy were used to determine the spatial organization of TRPV4 channels in arterial myocytes at a higher level of resolution than that of conventional confocal microscopy. The resolution of our GSD super-resolution localization maps was ∼30 nm. TIRF and super-resolution localization images of TRPV4 channels were acquired from the same cell. TRPV4 channels were labeled with a combination of primary and Alexa Fluor 647–conjugated secondary antibodies. The TIRF image in Fig. 1 B shows that TRPV4-associated fluorescence varied regionally, which suggests a nonhomogenous distribution of these channels within the sarcolemma of arterial myocytes. The super-resolution image of this cell showed that those zones of high fluorescence intensity in the TIRF image are produced by smaller TRPV4 channel puncta of various sizes (Fig. 1, B and C). The calculated areas of TRPV4 puncta followed an approximately exponential distribution with a mean of 454 ± 15 nm^2 (n = 28,652 clusters; Fig. 1 C). These confocal, TIRF, and super-resolution data suggest that TRPV4 channels are expressed along the sarcolemma of arterial myocytes, where they mostly form puncta of a wide range of sizes.

Elementary TRPV4 sparklets in arterial myocytes are produced by Ca^{2+} influx via single TRPV4 channels

Local Ca^{2+} signals resulting from the opening of TRPV4 channels ("TRPV4 sparklets") were recorded using TIRF microscopy in freshly isolated arterial myocytes and tsA-201 cells transiently expressing the TRPV4 channel (Fig. 2). In these experiments, cells were voltage-clamped

Downloaded from jgp.rupress.org on June 23, 2014

Published April 28, 2014

using the whole-cell configuration of the patch-clamp technique. Cells were imaged in the presence of 2 mM external Ca^{2+} while being held at −70 mV to increase the driving force for Ca^{2+} entry. $[Ca^{2+}]_i$ was monitored with the Ca^{2+} indicators Fluo-5F or Rhod-2.

We describe the experiments involving tsA-201 cells transiently expressing TRPV4 channels first. TRPV4 sparklets were recorded in tsA-201 before and after the application of the TRPV4-specific agonist GSK1016790A (GSK; 10 nM). Fig. 2 A shows a TIRF image of a representative cell and the time course of $[Ca^{2+}]_i$ in the area within the green circle under control conditions and after the application of GSK. TRPV4 sparklets were rarely observed under control conditions. However, application of 10 nM GSK evoked multiple TRPV4 sparklets in discrete regions of the cell. TRPV4 sparklets were not observed in nontransfected tsA-201 cells even in the presence of 10 nM GSK ($n = 5$). We generated an all-points histogram using TRPV4 sparklet records from multiple tsA-201 cells. The histogram had two distinct peaks and was fit with two Gaussian functions with centers at 0 and 50 nM corresponding to closed and open TRPV4 channels, respectively (Fig. 2 B).

In the next series of experiments, we recorded TRPV4 sparklets from freshly dissociated arterial myocytes in the absence and presence of GSK (Fig. 2 C). The experimental conditions were slightly different from those used to record TRPV4 sparklets in tsA-201 cells because cerebral artery myocytes express voltage-gated $Ca_V1.2$ channels, which are also capable of producing sparklets and could thus complicate our analysis. Accordingly, we implemented a multipronged approach to eliminate $Ca_V1.2$ channel activity. Myocytes were held at −70 mV, a membrane potential in which the open probability of $Ca_V1.2$ channels in arterial myocytes is low (Rubart et al., 1996). In addition, experiments were performed while cells were continuously exposed to an external solution containing 2 mM Ca^{2+} and the $Ca_V1.2$ channel antagonist nifedipine (1 µM). The use of 2 mM Ca^{2+} is important because at this concentration the vast majority of $Ca_V1.2$ sparklets are below the detection limit of our system. Thus, even if a few unblocked $Ca_V1.2$ channels manage to open in the presence of nifedipine, the $[Ca^{2+}]_i$ signals they will produce are unlikely to be detected.

Fig. 2 C shows a TIRF image of an arterial myocyte with two TRPV4 sparklet sites and the time course of $[Ca^{2+}]_i$ in one of these sites before and after the application of GSK. As in tsA-201 cells, TRPV4 sparklet activity under control conditions (i.e., nifedipine and no GSK) was low. A histogram of the amplitudes of TRPV4 sparklets recorded under control conditions has two peaks of decreasing amplitudes, which could be fit with a sum of two Gaussian functions with centers at 48 and 96 nM (Fig. 2 D). Thus, the quantal unit of Ca^{2+} influx via TRPV4 channels was ∼48 nM. We also quantified the duration of spontaneous TRPV4 sparklets in arterial myocytes (Fig. S1 A). TRPV4 sparklet duration had an exponential distribution with a time constant (τ) of 12 ± 1 ms (42 events).

Because TRPV4 channels in arterial myocytes have a lower sensitivity for GSK than heterologously expressed channels (Thorneloe et al., 2008), a higher concentration (100 nM) of this drug was used to activate TRPV4 sparklets in arterial myocytes. Application of 100 nM GSK increased TRPV4 sparklet activity by increasing the activity of previously active sites and recruiting new sites. The histogram of the amplitudes of TRPV4 sparklets in the presence of GSK could be fit with a sum of three Gaussian functions with centers at a $\Delta[Ca^{2+}]_i$ of 48, 96, and 144 nM. A histogram of the duration of TRPV4 sparklets in the presence of 100 nM GSK is shown

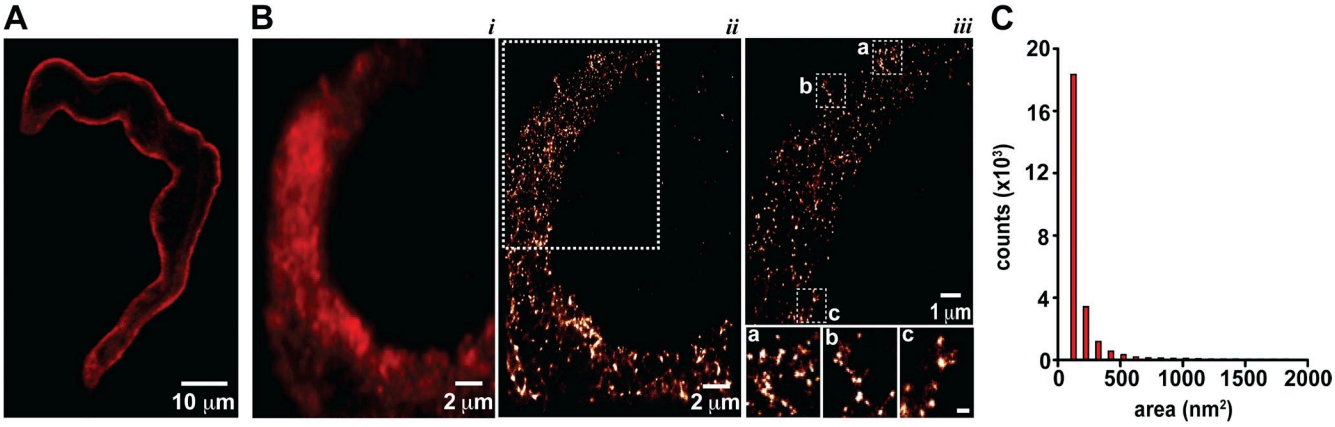

Figure 1. Super-resolution imaging reveals clustering of TRPV4 channels in arterial myocytes. (A) Confocal image of a representative arterial myocyte labeled with TRPV4-specific antibody and the corresponding secondary antibody. (B) TIRF image (i) and super-resolution localization maps (ii and iii) of an exemplar arterial myocyte labeled with a TRPV4-specific antibody. iii shows an expanded view of the region of the cell in ii marked by the rectangle. The insets in iii highlight TRPV4 channel clusters in regions a, b, and c of the myocyte. Inset bar, 200 nm. (C) Histogram of the area of TRPV4 channel clusters in super-resolution localization maps.

Downloaded from jgp.rupress.org on June 23, 2014

Published April 28, 2014

in Fig. S1 B. This histogram was fit with a sum of two exponential functions with a fast and slow τ of 12 ± 2 and 68 ± 7 ms (372 events), respectively. This analysis suggests that application of 100 nM GSK increased Ca^{2+} influx into arterial myocytes by increasing the duration and number TRPV4 sparklets without changing the amplitude of elementary TRPV4 sparklets (i.e., 48 nM).

We quantified the activity (nP_s) of TRPV4 sparklets in arterial myocytes under a broad range of experimental conditions (Fig. 2 E). Under control conditions, the nP_s of TRPV4 sparklets was 0.004 ± 0.002 (n = 31). In the presence of 3 nM or 100 nM GSK, TRPV4 sparklet activity in arterial myocytes was 0.03 ± 0.01 (n = 7) and 0.2 ± 0.02 (n = 31), respectively. The increase in

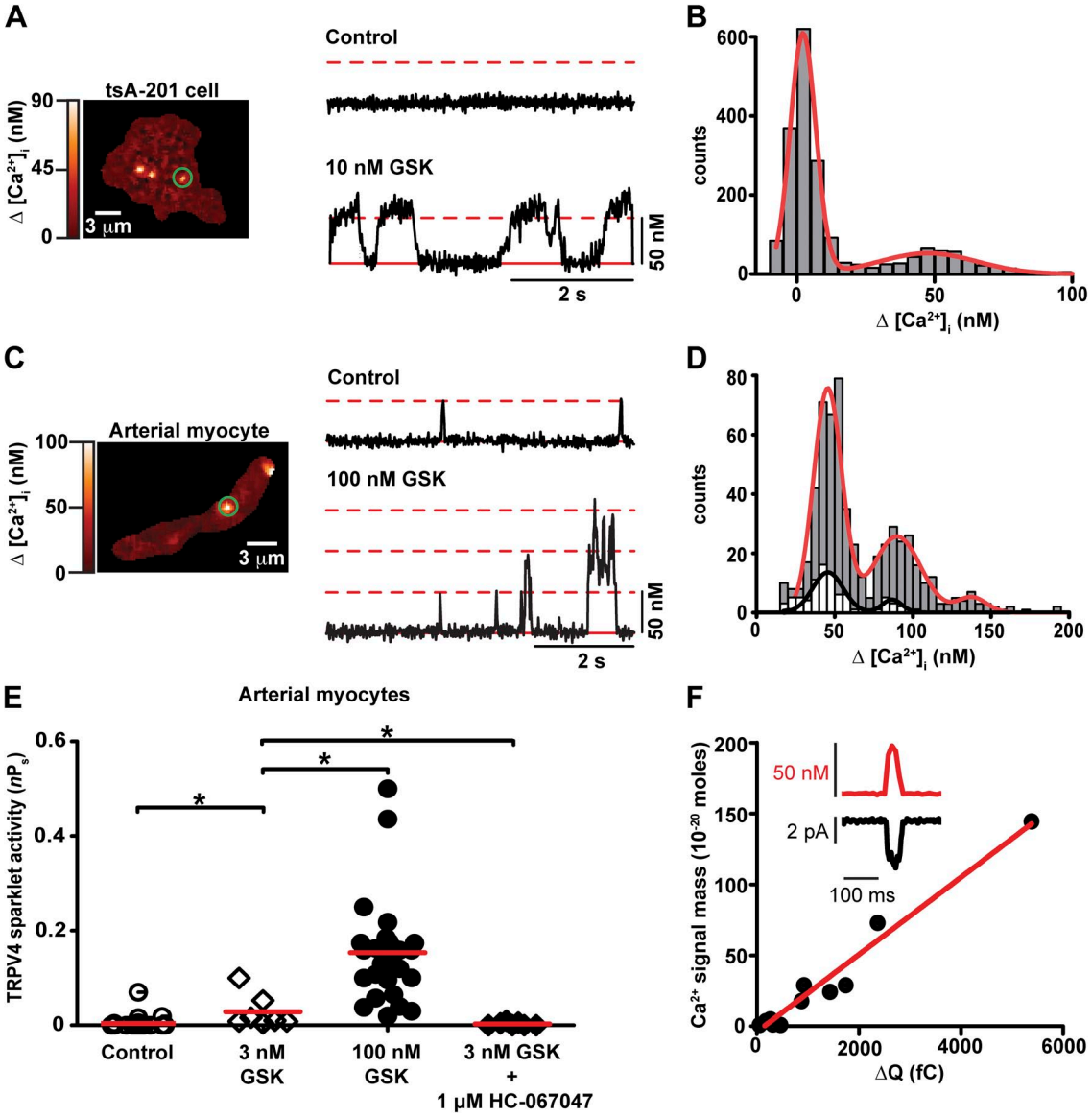

Figure 2. Elementary TRPV4 sparklets are produced by Ca^{2+} influx via single TRPV4 channels. (A) TIRF image of three sparklet sites in a representative tsA-201 cell expressing TRPV4 channels. The traces to the right of the image show time courses of $[Ca^{2+}]_i$ in the region of the cell marked by the green circle before and after the application of 10 nM GSK. The broken red line marks the amplitude of quantal TRPV4 sparklets. The solid red line highlights basal $[Ca^{2+}]_i$. (B) All-points histogram of TRPV4 sparklets after GSK application. The red line is the best fit to the data using a multi-Gaussian function with a q value of 48 nM. (C) TIRF image of a representative arterial myocyte and time courses of $[Ca^{2+}]_i$ within the area of the cell demarcated by the green circle before and after exposure to 100 nM GSK. (D) Histogram of the amplitudes of TRPV4 sparklets before (white bars) and after (gray bars) GSK application. Data were fit (solid lines) with a multi-Gaussian function (q = 48 nM). (E) Scatter plot of TRPV4 sparklet activity in arterial myocytes. The red lines are the median values. *, $P < 0.05$; Mann-Whitney test. (F) Plot of the relationship between TRPV4 sparklet signal mass and ΔQ_{TRPV4} in arterial myocytes. The solid line is a linear fit to the data ($r^2 = 0.97$). The inset shows a simultaneous recording of a TRPV4 current (black) and sparklet (red) from an arterial myocyte.

Downloaded from jgp.rupress.org on June 23, 2014

Published April 28, 2014

TRPV4 sparklet activity induced by GSK was reversed by the application of the selective TRPV4 channel antagonist HC-0670473 (HC; 1 µM; nP_s = 0.003 ± 0.001, n = 7; Fig. 2 E). We also investigated the effects of the physiological TRPV4 channel activator 11,12-EET (300 nM) on sparklets. Importantly, the physiological TRPV4 channel activator 11,12-EET induced a nearly 50-fold increase in TRPV4 sparklet activity (nP_s = 0.20 ± 0.05, n = 10) above control levels.

Having established that native and heterologously expressed TRPV4 channels produce sparklets of similar amplitudes and pharmacological profiles, we tested the hypothesis that quantal TRPV4 sparklets are produced by the opening of single TRPV4 channels in arterial myocytes (Fig. 2 F). To test this hypothesis, we simultaneously recorded TRPV4 currents and sparklets in arterial myocytes. Because basal TRPV4 channel activity is very low, experiments were performed in the presence of 3 nM GSK. We used this relatively low concentration of GSK to induce a small increase in the open probability of TRPV4 channels, but to a level where most currents and sparklets are produced by the opening of a single TRPV4 channel.

The inset in Fig. 2 F shows a simultaneously recorded TRPV4 current and sparklet. At −70 mV, the amplitude of TRPV4 currents we recorded was −3.68 ± 0.41 pA (n = 16 cells), which are similar to those recorded by others from single TRPV4 channels under comparable experimental conditions (Strotmann et al., 2000; Watanabe et al., 2003; Cao et al., 2009). Inward TRPV4 currents were always associated with sparklets with amplitudes similar to those of quantal TRPV4 sparklets in tsA-201 and arterial smooth muscle cells (i.e., ∼48 nM Ca^{2+}; Fig. 2 F, inset). We determined the signal mass of TRPV4 sparklets to quantify the total amount of Ca^{2+} influx associated with each event. This value was linearly correlated (r^2 = 0.97) to the amount of charge movement (in coulombs) associated with the simultaneously recorded TRPV4 current (Q_{TRPV4}; Fig. 2 F), providing further support to the hypothesis that single TRPV4 channel currents mediate elementary TRPV4 sparklets.

The amount of Ca^{2+} entering an arterial myocyte during a TRPV4 sparklet is larger than that during a $Ca_V1.2$ sparklet

As mentioned previously, myocytes from resistance arteries express TRPV4 and $Ca_V1.2$ channels, both capable of conducting Ca^{2+} and eliciting sparklets. However, whereas $Ca_V1.2$ channels are the preponderant source of Ca^{2+} for contraction, TRPV4 channels have been linked to relaxation (Harder et al., 1987; Fleischmann et al., 1994; Rubart et al., 1996; Jaggar et al., 1998; Earley et al., 2005, 2009; Navedo et al., 2005; Amberg et al., 2007). The functional role of TRPV4 and $Ca_V1.2$ sparklets could be caused by differences in Ca^{2+} influx through these channels in arterial myocytes. To test this hypothesis, we compared the amplitude and signal mass of sparklets elicited by TRPV4 and $Ca_V1.2$ channels (Fig. 3). As described earlier, all recordings were performed while arterial myocytes were superfused with a saline solution containing 2 mM Ca^{2+} and held at −70 mV. $Ca_V1.2$ sparklets were identified as nifedipine-sensitive Ca^{2+} influx events while TRPV4 sparklets were identified as nifedipine-insensitive sparklets that increased upon application of GSK.

Panels A and B in Fig. 3 show all-point histograms of TRPV4 and $Ca_V1.2$ sparklets in arterial myocytes, respectively. The TRPV4 sparklet histogram shows two peaks at 0 (i.e., baseline, closed channels) and 48 nM (i.e., open channel). However, the $Ca_V1.2$ sparklets histogram exhibited $\Delta[Ca^{2+}]_i$ amplitudes at 0 and close to our amplitude detection threshold of 18 nM. This suggests that with 2 mM external Ca^{2+}, many $Ca_V1.2$ sparklets cannot be detected with our system. Thus, the amplitude of TRPV4 sparklets is larger than that of $Ca_V1.2$ sparklets at physiological Ca^{2+} levels. Indeed, we found that

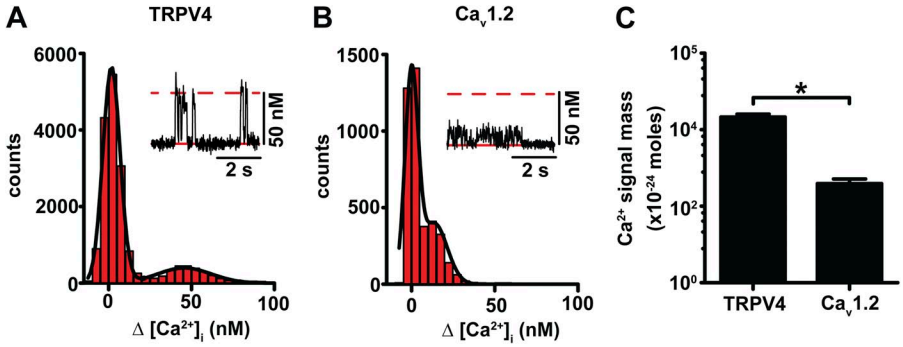

Figure 3. The amplitude of the signal mass of quantal TRPV4 sparklets is larger than that of $Ca_V1.2$ sparklets under physiological extracellular Ca^{2+} conditions. (A and B) All-points histograms generated from TRPV4 (A) and $Ca_v1.2$ (B) sparklet records from arterial myocytes. The solid black lines represent best fits to the data with a multi-Gaussian function for TRPV4 (q = 48 nM) and $Ca_v1.2$ (q = 18 nM) sparklets. The insets show representative TRPV4 and $Ca_v1.2$ sparklet records (membrane potential = −70 mV; external Ca^{2+} = 2 mM). The broken red lines in the insets mark the amplitude of quantal TRPV4 sparklets. The solid red lines highlight basal $[Ca^{2+}]_i$. TRPV4 sparklets were recorded in the presence of 100 nM GSK. (C) Bar plot of the Ca^{2+} signal mass of $Ca_v1.2$ (92 events) and TRPV4 (15 events) sparklets in arterial myocytes. Data are means ± SEM (error bars; *, P < 0.05; two-tailed Student's t test).

Downloaded from jgp.rupress.org on June 23, 2014

Published April 28, 2014

the signal mass of TRPV4 sparklets was ~100-fold larger than that of $Ca_V1.2$ sparklets (Fig. 3 C).

Because in the presence of 2 mM Ca^{2+} many $Ca_V1.2$ sparklets fall below the detection limit of our system, their activity cannot be accurately estimated under these experimental conditions. Thus, we recorded $Ca_V1.2$ sparklet activity in the presence of 20 mM external Ca^{2+}, which allowed us to record elementary $Ca_V1.2$ sparklets with an amplitude of ~40 nM (Fig. S2). Analysis of these records revealed that basal $Ca_V1.2$ sparklet activity (nP_s = 0.095 ± 0.030) was higher than TRPV4. Thus, although Ca^{2+} influx through individual TRPV4 channels is higher than that of $Ca_V1.2$ channels, the mean $Ca_V1.2$ sparklet activity at −70 mV is ~24-fold higher than that of TRPV4 sparklets (nP_s = 0.004 ± 0.020) in cerebral arterial myocytes. Note that membrane depolarization from −70 mV to the physiological membrane potential −40 mV should amplify this difference in $Ca_V1.2$ and TRPV4 sparklet activity, as the open probability of $Ca_V1.2$, but not TRPV4 channels, increases exponentially over this voltage range (Rubart et al., 1996).

AngII increases TRPV4 sparklet activity in arterial myocytes

We used the biophysical data described to study the mechanisms by which physiological signals control TRPV4-mediated Ca^{2+} entry in arterial myocytes. We focused on the vasoconstrictor AngII because it is an important regulator of myocyte contraction, arterial diameter, and blood pressure. Furthermore, binding of AngII to its receptor activates a signaling cascade that culminates in the activation of PKC in arterial myocytes, and activation of this kinase seems to increase the activity of TRPV4 channels in neurons (Cao et al., 2009). At present, however, whether activation of AngII-PKC signaling modulates TRPV4 channel function in arterial myocytes is unknown. Thus, we tested the hypothesis that AngII increases TRPV4 sparklet activity in arterial myocytes. Because AngII can activate $Ca_V1.2$ and TRPV4 sparklets, we used a pharmacological fingerprinting approach to distinguish between these two events, identifying nifedipine-sensitive, HC-resistant events as $Ca_V1.2$ sparklets and nifedipine-resistant, HC-sensitive events as TRPV4 sparklets (Fig. S2). All recordings were performed at physiological Ca^{2+} concentrations (2 mM).

Application of 100 nM AngII increased sparklet activity. Nearly 70% of these Ang-induced sparklet events were eliminated by application of an extracellular solution containing 1 µM nifedipine. The nifedipine-sensitive sparklets (presumably $Ca_V1.2$ sparklets) had amplitudes ranging from 18 to 30 nM. Subsequent exposure to a solution containing nifedipine and the selective TRPV4 channel antagonist HC (1 µM) eliminated all remaining sparklet events (~30%; Fig. S2 C). Collectively, these data suggest that, under these conditions, TRPV4 sparklets accounted for ~30% of the total sparklet events induced by AngII in arterial myocytes (Fig. S2 C).

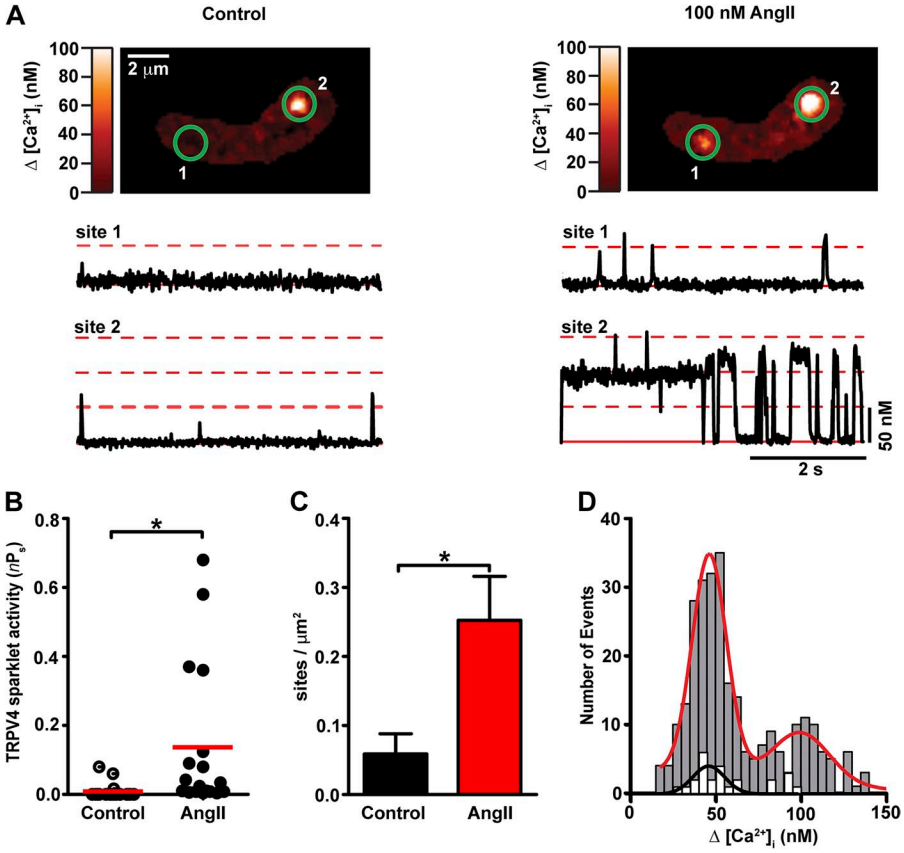

Figure 4. AngII increases TRPV4 sparklet activity in arterial myocytes. (A) TIRF images of an arterial myocyte before (left) and after (right) application of 100 nM AngII. The traces below each image show the time course of $[Ca^{2+}]_i$ in sites 1 and 2. Broken red lines mark the amplitude of elementary and multichannel TRPV4 sparklets, whereas the solid line shows the baseline. (B) Scatter plot of TRPV4 sparklet activity under control conditions and after application of AngII. The red lines are the median values (*, $P < 0.05$; $n = 18$; Mann-Whitney test). (C) Bar plot of TRPV4 sparklet site density before and after application of AngII. Data are means ± SEM (error bars; *, $P < 0.05$, $n = 4$; two-tailed Student's t test). (D) Amplitude histogram of TRPV4 sparklets before (white bars) and after AngII (gray bars) application. Data were fit with a Gaussian function with a q-value of 48 nM for control (black line) and AngII (red line) data.

Downloaded from jgp.rupress.org on June 23, 2014

Published April 28, 2014

To resolve $Ca_V1.2$ sparklets with amplitudes near or below the detection threshold (18 nM), we imaged cells after increasing the extracellular concentration of Ca^{2+} from 2 to 20 mM, but in the presence of the TRPV4 channel antagonist HC (1 µM). As shown in Fig. S2 D, 100 nM AngII increased $Ca_V1.2$ sparklet activity to a level similar to that reported by Navedo et al. (2008).

AngII modulated TRPV4-mediated Ca^{2+} influx by increasing TRPV4 sparklet activity and density ∼15-fold and ∼5-fold, respectively (Fig. 4, A–C). A histogram of TRPV4 sparklet duration could be fit by the sum of two exponential functions with fast (τ_{fast}) and slow (τ_{slow}) time constants of 12 ± 1 ms to 69 ± 8 ms, respectively (252 events; Fig. S1 C). The TRPV4 sparklets with long durations (i.e., t_{slow}) that occurred in the presence of AngII were not observed under control conditions (i.e., no AngII; Fig. S1 A). A histogram of TRPV4 sparklet amplitudes before and after the application of AngII illustrates that AngII increased the number of TRPV4 sparklet events without changing the amplitude of elementary events (i.e., 48 nM Ca^{2+}; Fig. 4 D). Thus, AngII increases TRPV4-mediated Ca^{2+} influx in arterial myocytes by increasing the duration of individual TRPV4 sparklets as well as the probability of TRPV4 sparklet occurrence.

TRPV4 channels oppose AngII-induced vasoconstriction

In arterial smooth muscle cells, TRPV4 channels are proposed to form part of a signaling pathway that upon activation causes relaxation via the activation of large conductance Ca^{2+}-activated K^+ channels in the cells (Earley et al., 2005). A testable prediction of this hypothesis is that application of AngII will induce a larger vasoconstriction in arteries from TRPV4-null ($TRPV4^{-/-}$) than from WT mice. To test this hypothesis, cerebral resistance arteries from WT and $TRPV4^{-/-}$ mice were cannulated, denuded from their endothelium, and pressurized to an intravascular pressure of 60 mmHg. Arterial diameter was measured under control conditions and after the application of AngII. AngII-induced constrictions were normalized to the constriction induced by 100 nM of the thromboxane A2 receptor agonist U41169. Fig. 5 A shows arterial diameter traces from representative WT and $TRPV4^{-/-}$ arteries. Application of U41169 (100 nM) constricted WT and $TRPV4^{-/-}$ arteries to the same extent, which suggests that loss of TRPV4 does not alter thromboxane A2 signaling in smooth muscle. Note, however, that application of 100 pM AngII evoked a stronger vasoconstriction in $TRPV4^{-/-}$ than in WT arteries.

The plot in Fig. 5 B shows the effects of a broader range of AngII concentrations on arterial diameter. The AngII concentration–vasoconstriction relationship of WT and $TRPV4^{-/-}$ arteries was sigmoidal. The effective AngII concentration required to evoke a vasoconstriction that is 50% of the maximal constriction response to U41169 (i.e., EC_{50}) in $TRPV4^{-/-}$ (4.7×10^{-11} M) and WT (6.6×10^{-11} M) arteries was comparable. This suggests that the number or sensitivity of AngII receptors in these arteries is similar. Importantly, and consistent with our hypothesis, AngII induced greater constrictions in $TRPV4^{-/-}$ than in WT arteries at concentrations >100 pM (Fig. 5). Thus, TRPV4 channels form part of signaling pathway that opposes AngII-induced vasoconstriction of cerebral arteries.

Optogenetic and pharmacological approaches suggest that PKC is required for AngII-induced increases in TRPV4 sparklet activity in arterial myocytes

We tested the hypothesis that AngII increases TRPV4 sparklet activity through activation of PKC. To do this, we used complementary pharmacological and optogenetic approaches. First, we examined the effects of AngII on TRPV4 sparklets before and after the application of the PKC inhibitor Gö6976 (Fig. 6). Application

Downloaded from jgp.rupress.org on June 23, 2014

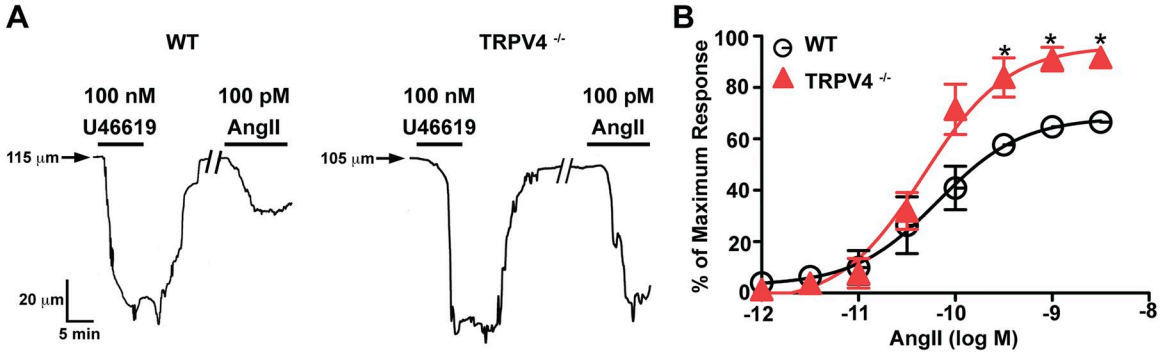

Figure 5. TRPV4 channels oppose AngII-induced artery constriction. (A) Internal diameter records WT (right) and $TRPV4^{-/-}$ (left) arteries pressurized to 60 mmHg. Solid horizontal bars mark the time when arteries were exposed to U46619 (100 nM) and AngII (100 pM). The forward slashes (//) in the traces indicate a gap of 15 min. (B) Plot of the percentage of the maximum vasoconstriction (AngII-induced contraction/U46619-induced contraction × 100) induced by application of various AngII concentrations to WT ($n = 4$) and $TRPV4^{-/-}$ ($n = 3$) arteries. Solid lines are fits to the data with a dose–response function Y = maximal response + (maximal response − minimal response)/$(1 + 10^{LogEC50 - X})$. Data are means ± SEM (error bars; *, $P < 0.05$; two-tailed Student's t test).

Published April 28, 2014

of Gö6976 (100 nM) significantly decreased AngII-induced TRPV4 sparklet activity in arterial myocytes (Fig. 6, A and B), which suggests that PKC is necessary for AngII-dependent stimulation of TRPV4 sparklets.

Second, we took advantage of optoXRs, a new family of opsin-GPCR chimeras (Airan et al., 2009). We used a chimera formed by fusion of the intracellular loops of the human α_{1a}-adrenergic receptor with the transmembrane domains of opsin. The result is a light-sensitive protein termed "opto-α_1AR" that can be activated with precise temporal and spatial control to initiate G_q-mediated synthesis of DAG and IP_3. Opto-α_1AR was fused to YFP to facilitate identification of transfected cells and to allow determination of the localization of this light-sensitive protein within the cell.

As shown in the confocal image in Fig. 6 C (i), opto-α_1AR is broadly expressed along the surface membrane of tsA-201 cells. To monitor $[Ca^{2+}]_i$, cells were loaded with the Ca^{2+} indicator Rhod-2. Areas of photoactivation of opto-α_1AR ranged from 3 to 12 μm^2. To prevent Ca^{2+} release from intracellular stores via IP_3 receptors, xestospongin C (3 µM) was included in the patch pipette solution used in these experiments. As a control, we investigated the effects of local 474 nm light illumination on $[Ca^{2+}]_i$ in cells expressing opto-α_1AR and PKCα only (Fig. 6 C, ii; $n = 3$). Illumination of two randomly selected sites with 473 nm light for 1 min did not evoke a change in $[Ca^{2+}]_i$ in these cells. A similar experiment was performed in cells expressing TRPV4 channels, PKCα, and opto-α_1AR. In these cells, local light-induced activation of opto-α_1AR elicited large local increases in $[Ca^{2+}]_i$ wherever protein was located (Fig. 6 C, iii; $n = 3$).

Having shown that local activation of G_q-mediated signaling increases $[Ca^{2+}]_i$, presumably via activation of TRPV4 channels (Fig. 6 C), we investigated the effects of global, cell-wide activation of opto-α_1AR on TRPV4 currents. Fig. 6 D shows TRPV4 currents recorded during a voltage ramp from −100 to +120 mV before and after illumination with 473 nm light. Consistent with the Ca^{2+} data, global, cell-wide illumination of cells with 473 nm light (1 min) increased whole-cell TRPV4 currents twofold (Fig. 6, D and E).

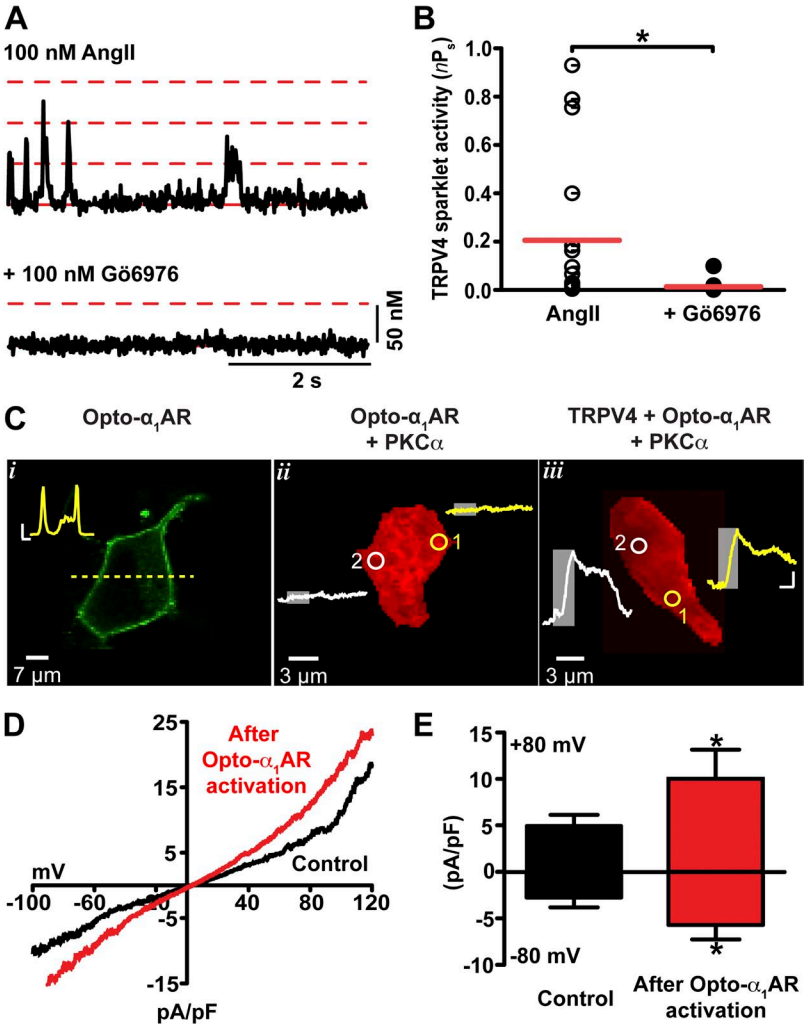

Figure 6. AngII increases TRPV4 sparklet activity through the local activation of PKC. (A) Representative $[Ca^{2+}]_i$ records from a TRPV4 sparklet site in an arterial myocyte exposed to AngII (100 nM) or AngII plus Gö6976 (100 nM). Broken red lines mark the amplitude of elementary and multichannel TRPV4 sparklets; the solid line shows the baseline. (B) Scatter plot of TRPV4 sparklet activities under the experimental conditions shown in A. The red lines are the median values (*, $P < 0.05$; $n = 17$; Mann-Whitney test). (C) Confocal images of tsA-201 cells expressing opto-α_1AR (i), opto-α_1AR + PKCα (ii), or TRPV4 + opto-α_1AR + PKCα (iii). (i) Image of a tsA-201 showing opto-α_1AR-YFP membrane localization. The inset shows the fluorescence intensity along the yellow dashed line. Inset bars: (horizontal) 2 µm; (vertical) 10 AU. (ii and iii) Ca^{2+} imaging of tsA-201 cells expressing opto-α_1AR + PKC (ii) or TRPV4 + opto-α_1AR + PKC (iii), and loaded with the Ca^{2+} indicator Rhod-2. The traces in ii and iii show the time course of $[Ca^{2+}]_i$ in sites 1 and 2. The gray rectangles on the traces show when opto-α_1AR was stimulated with 474 nm light in sites 1 and 2. Bars in traces: (horizontal) 20 s; (vertical) 1,000 AU. (D) Representative TRPV4 whole-cell currents of tsA-201 cells coexpressing TRPV4 channels, PKCα, and opto-α_1AR before (black line) and after (red line) cell-wide opto-α_1AR activation (60 s with 474 nm light). (E) Bar plot of the amplitude of TRPV4 currents at −80 mV and +80 mV before and after opto-α_1AR activation. Data are means ± SEM (error bars; *, $P < 0.05$; $n = 6$; one-tailed Student's t test).

Downloaded from jgp.rupress.org on June 23, 2014

Published April 28, 2014

AKAP150 is required for AngII-induced increases in TRPV4 sparklet activity in arterial myocytes

The data presented raise an important question: if TRPV4 channels are activated by PKC and functional channels are expressed broadly along the membrane, why is TRPV4 sparklet activity restricted to only a few sites within the membrane? One potential explanation is that the anchoring protein AKAP150 targets PKC to sarcolemmal microdomains, where it selectively modulates nearby TRPV4 channels.

A prediction of this hypothesis is that AKAP150 is required for AngII-induced increases in TRPV4 sparklet activity. To test this prediction, we imaged TRPV4 sparklets in arterial myocytes isolated from WT and AKAP150$^{-/-}$ mice (Fig. 7, A and B). Although basal TRPV4 sparklet activity was low in WT arterial myocytes, these events were never observed in AKAP150$^{-/-}$ myocytes. This was not caused by a reduced expression of the channels in AKAP150$^{-/-}$ myocytes, as GSK increased TRPV4 sparklet activity (Fig. 7 A and B) and TRPV4 mRNA was detected (Fig. 7 C) in these cells. Furthermore, although GSK increased TRPV4 sparklet activity to a larger extent in WT than AKAP150$^{-/-}$ myocytes (Fig. 7 B), we found that application of 100 nM AngII increased TRPV4 sparklets in WT, but not AKAP150$^{-/-}$ myocytes (Fig. 7, D and E). The amplitude of elementary TRPV4 sparklet events was similar in WT and AKAP150$^{-/-}$ myocytes (Fig. 7 F). Together, these findings suggest that AKAP150 is required for modulation of TRPV4 sparklet activity in arterial myocytes during AngII signaling.

The interactions between AKAP150 and TRPV4 channels are dynamic

Although TRPV4 and AKAP79 (the human orthologue of AKAP150) have been shown to coimmunoprecipitate (Zhang et al., 2008), there is no direct evidence indicating that they interact in cells. This is important because in living cells the number and strength of AKAP150–TRPV4 interactions could be under the control of multiple physiological processes. To address this critical issue, we implemented a combination of confocal and super-resolution imaging approaches to determine the mobility, temporal dynamics, and localization of AKAP150 and TRPV4 channels.

FRAP was used to determine the fraction of mobile and immobile TRPV4-mCherry and AKAP150-EGFP expressed in tsA-201 cells. Photobleaching was limited to an area of ~3–12 μm^2 of the surface membrane (i.e., ~0.1–0.2% of the surface area of a tsA-201 cell). Fig. 8 A shows the results of a FRAP experiment in a cell expressing AKAP150-EGFP. AKAP150-associated fluorescence decreased to nearly zero after illumination with high intensity light. After this, AKAP150-GFP increased with a seemingly exponential time course to only ~60% of the prebleaching (i.e., control) fluorescence intensity, which suggests that a fraction of AKAP150 is immobile. Similar FRAP recoveries were obtained for TRPV4-mCherry (Fig. 8 B). These data suggest that TRPV4-mCherry and AKAP150-EGFP have mobile (i.e., recovered fluorescence) and seemingly immobile (i.e., unrecovered fluorescence) fractions in tsA-201 cells.

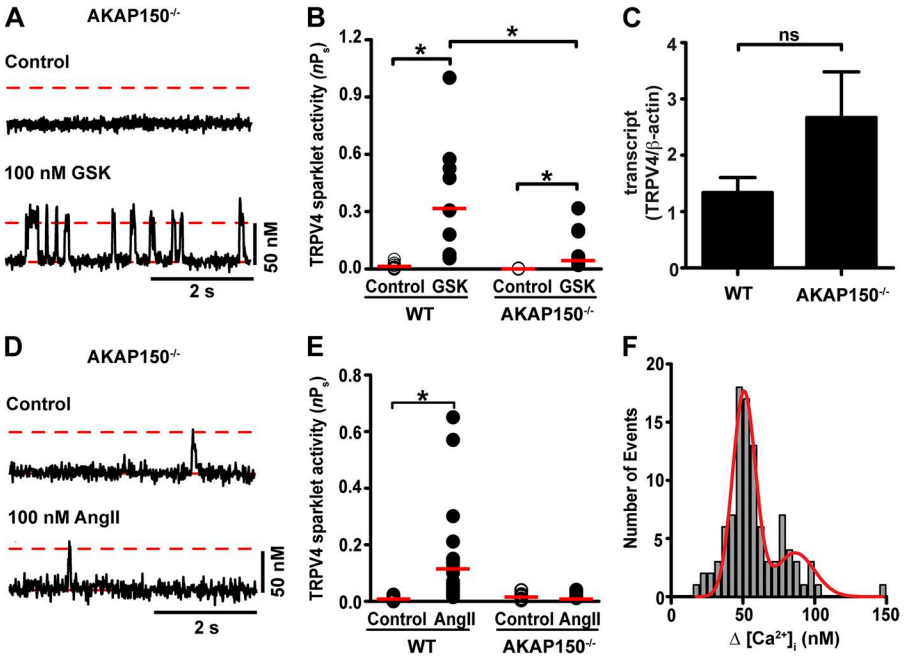

Figure 7. AKAP150 is required for AngII-induced, PKC-dependent regulation of TRPV4 sparklet activity in arterial myocytes. (A) Representative records of $[Ca^{2+}]_i$ from a TRPV4 sparklet site before (top) and after (bottom) application of 100 nM GSK in an AKAP150$^{-/-}$ arterial myocyte. The broken red lines show the amplitude of elementary TRPV4 sparklets. Solid red lines highlight basal $[Ca^{2+}]_i$. (B) Scatter plot of the activities of TRPV4 sparklet sites under control conditions and after application of GSK in WT (n = 10) and AKAP150$^{-/-}$ (n = 25) arterial myocytes. The red lines are the median values (*, P < 0.05; Mann-Whitney test). (C) Bar plot of the normalized (TRPV4/β-actin) TRPV4 transcript level in WT and AKAP150$^{-/-}$ myocytes (n = 3). Data are means ± SEM (error bars). ns, not significant. (D) TRPV4 sparklet records from an AKAP150$^{-/-}$ myocyte before and after application of 100 nM AngII. (E) Scatter plot of TRPV4 sparklet activities in WT (n = 23) and AKAP150$^{-/-}$ (n = 13) myocytes in the absence (control) and presence of AngII. The red lines are the median values (*, P < 0.05; Mann-Whitney test). (F) Histogram of the amplitudes of TRPV4 sparklets before and after exposing AKAP150$^{-/-}$ arterial myocytes to GSK. The red line is the best fit to the GSK data with a Gaussian function using a q value of 48 nM.

Downloaded from jgp.rupress.org on June 23, 2014

Published April 28, 2014

Next, we used RICS to quantify the diffusion coefficients of TRPV4-mCherry and AKAP150-EGFP. ccRICS was used to examine AKAP150–TRPV4 interactions in detail (Digman et al., 2009a,b; Rossow et al., 2010). Because these techniques are relatively new, we will describe them briefly before describing the results of our experiments. In RICS and ccRICS, pixel intensities are collected sequentially from left to right, row by row until an entire image (256 × 256 pixels) is obtained. Scanner fly-back and pixel dwell times are taken into account to obtain temporal information about fluorescence intensity fluctuations from the image. Image correlations were fit with an equation relating the correlation to the diffusion coefficient of the fluorescent proteins imaged. The shape of the resulting RICS function reflects the diffusion rate and binding interactions between proteins. For example, the RICS function of rapidly diffusing fluorescent proteins typically has an elongated shape along the fast scan axis (i.e., x axis) because molecules move fast relative to the line scanning time. In contrast, the RICS cross-correlation function of slow (relative to the x axis) protein–protein interactions is typically round in shape because of a high probability of correlating particles in the x axis and slower y axis.

We collected images from the center and top of cells expressing TRPV4-mCherry and AKAP150-EGFP (Fig. 8 C). Results obtained from the analysis of an exemplar cell are shown in Fig. 8 D. The value $G(x,y)$ is the correlation function and x and y the spatial correlation shifts. We found that the diffusion coefficient of TRPV4 (D_{TRPV4} = 1.0 ± 0.3 μm^2/s) was faster than that of AKAP150 (D_{AKAP} = 0.6 ± 0.2 μm^2/s; n = 8, P < 0.05). Furthermore, our ccRICS analysis suggests that the diffusion coefficient (D_{CC}) of correlated AKAP150 and TRPV4 channels was 0.8 ± 0.2 μm^2/s (n = 8).

We tested the hypothesis that AKAP150 and TRPV4 channels dynamically interact in the surface membrane using ccRICS. If the movement of AKAP150 and TRPV4 is correlated, as expected if these proteins were to interact in the membrane, the amplitude of their cross-correlation function (G_{cc}) could be, at most, similar to the amplitude of the autocorrelations (G_{TRPV4} or G_{AKAP}). Cross-correlation values significantly lower than G_{TRPV4} or G_{AKAP} would imply that the movement of these molecules is uncorrelated. Consistent with our hypothesis, the ccRICS function of TRPV4 and AKAP150 was large in amplitude and round in shape (Fig. 8 D). Indeed, the cross-correlation ratio of AKAP150 and TRPV4 (G_{cc}/[mean of G_{TRPV4} and G_{AKAP}]) was 0.40 ± 0.05 (n = 8).

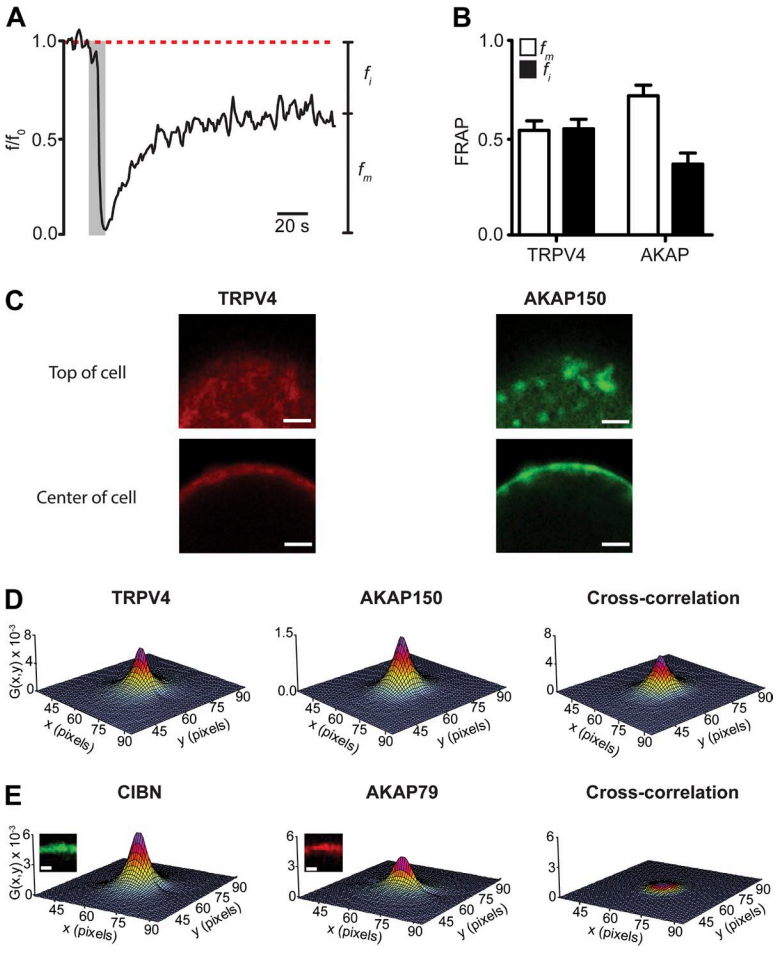

Figure 8. The interactions between AKAP150 and TRPV4 channels are dynamic. (A) FRAP of AKAP150-EGFP in a small region of interest (diameter = 1 μm) of a representative tsA-201 cell. The gray rectangle shows the bleaching period with high-intensity 474 nm light. The broken line marks the mean AKAP150-EGFP fluorescence intensity before bleaching. f_m and f_i are mobile and immobile fractions, respectively. (B) Bar plots of the mobile and immobile fractions. Data are means ± SEM (error bars; n = 5). (C) Confocal images of the top and center of a cell expressing TRPV4-mCherry and AKAP150-EGFP. Bars, 2 μm. (D) RICS auto (TRPV4 and AKAP150) and cross-correlation (ccRICS) signal. (E) RICS auto (CIBN and AKAP79) and cross-correlation (ccRICS) signal. Bars, 2 μm.

Downloaded from jgp.rupress.org on June 23, 2014

Published April 28, 2014

This cross-correlation ratio is nearly eightfold higher than that of membrane-associated AKAP150-mCherry and CIBN-EGFP-CAAX (0.05 ± 0.02; $n = 3$), which presumably do not interact (Fig. 8 E). CIBN-EGFP-CAAX was generated by fusing the transcription factor CIBN to EGFP and by adding a CAAX box to its C terminus to ensure plasma membrane targeting of this protein (Idevall-Hagren et al., 2012). Collectively, our ccRICS data suggest that the correlated movements of TRPV4 and AKAP150 are likely caused by specific localized interactions between these proteins in the surface membrane.

Having found that AKAP150 and TRPV4 channels interact in the surface membrane of tsA-201 cells, we investigated the spatial organization of these two proteins in arterial myocytes using confocal and super-resolution imaging. As illustrated in the confocal image in Fig. 9 A, AKAP150 (green) and TRPV4 channels (red) are expressed along the sarcolemma of arterial myocytes. The Pearson correlation coefficient between the AKAP150 and TRPV4-associated fluorescence signals was +0.91, which indicates that a large fraction of these proteins are separated by <250 nm in arterial myocytes (Fig. 9 A).

Super-resolution GSD localization maps of AKAP150 indicate that, like TRPV4, this protein is not homogeneously distributed along the sarcolemma of arterial myocytes. Rather, AKAP150 is expressed in small puncta with a mean area of 2,300 ± 82 nm^2 ($n = 53{,}531$ particles). Analysis of super-resolution localization maps from cells labeled with TRPV4 and AKAP150 antibodies indicated that only a small fraction (~1.3%) of AKAP150 puncta were <30 nm away from TRPV4 channel puncta in arterial myocytes (Fig. 9, B and C).

We demonstrated that AngII modulates TRPV4-mediated Ca^{2+} influx by increasing TRPV4 activity of previous active sites and by forming new sites. Because AKAP150 and TRPV4 can move within the surface

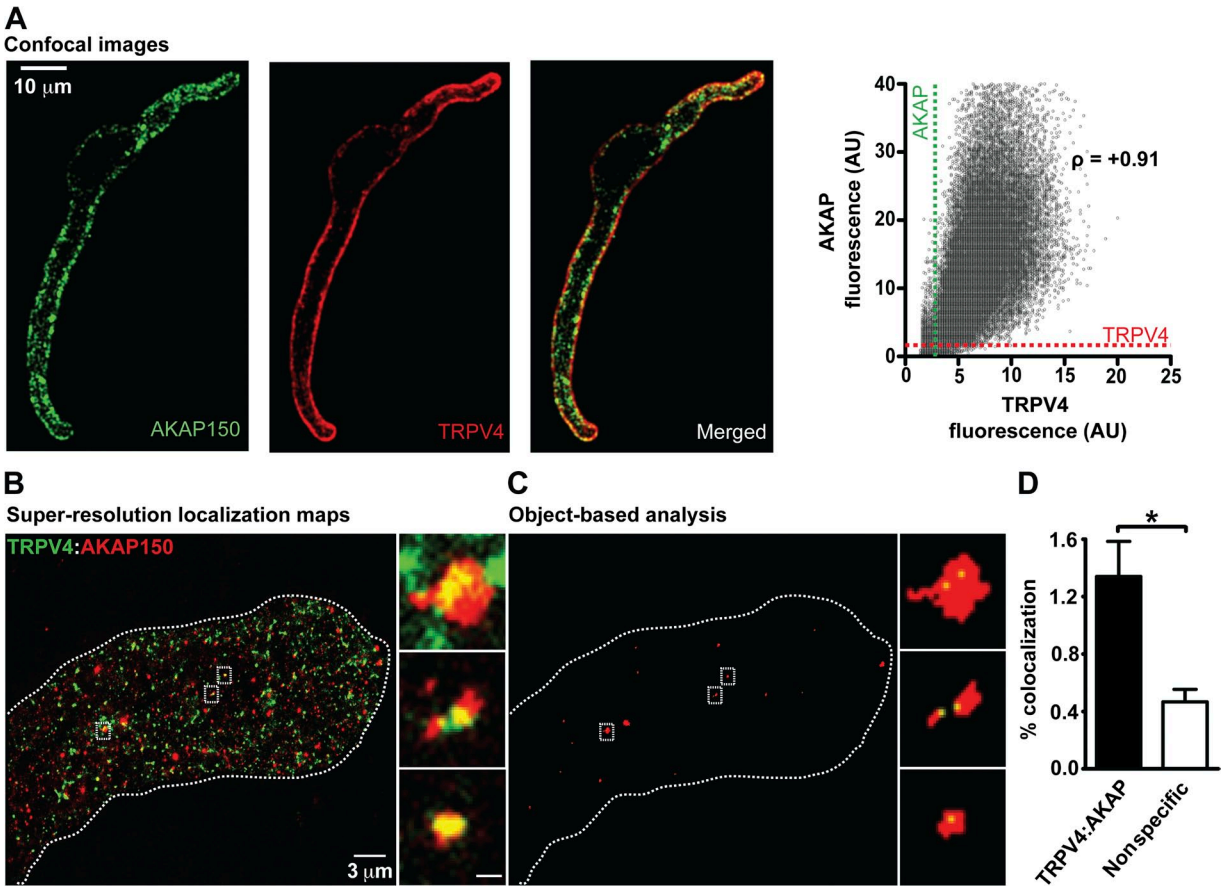

Figure 9. Spatial organization of AKAP150 and TRPV4 channels in arterial myocytes. (A) Confocal immunofluorescence images of AKAP150 and TRPV4 in an arterial myocyte. The image to the right was generated by merging the AKAP150 and TRPV4 images. The graph shows the relationship between TRPV4 and AKAP150-associated fluorescence for each pixel in these images. The broken lines show the thresholds for signal detection in the AKAP150 and TRPV4 channel. The Pearson's coefficient (ρ) was +0.91. (B) Super-resolution localization map of TRPV4 (green) and AKAP150 (red) in an arterial myocyte. (C) Regions where TRPV4 (green) and AKAP150 (red) colocalized in the super-resolution map in B after object-based colocalization analysis. Insets in B and C are enlarged views of the regions of the cells marked by the rectangles. The broken lines mark the outline of the cell. Inset bar, 200 nm. (D) Percentage of TRPV4 channels showing specific and nonspecific (i.e., random) colocalization within 30 nm of AKAP150. Data are means ± SEM (error bars; *, $P < 0.05$; $n = 4$; one-tailed Student's t test).

Downloaded from jgp.rupress.org on June 23, 2014

Published April 28, 2014

membrane of cells, we tested the hypothesis that AngII increases the proximity between TRPV4 and AKAP150 complexes. Consistent with our hypothesis, we found that activation of AngII signaling increased the proximity of AKAP150 and TRPV4 puncta in arterial myocytes. Indeed, there was an approximately threefold increase in the fraction of AKAP150 and TRPV4 at or below 30 nm in arterial myocytes (Fig. S3). This suggests that, as in tsA-201 cells, AKAP150 and TRPV4 channels move and could increase their proximity in the sarcolemma of arterial myocytes.

DISCUSSION

Our data support a new model for the local regulation of Ca^{2+} influx via TRPV4 channels in arterial myocytes (Fig. 10). In this model, the opening of TRPV4 channels results in large amplitude sparklets. Although basal TRPV4 sparklet activity is low, activation of G_q-coupled AngII receptors as well as application of the channel activator GSK and 11,12-EET boost Ca^{2+} influx by increasing the amplitude, frequency, and duration of TRPV4 sparklets. Our data indicate that AKAP150 and PKC are required for the enhancement of TRPV4 sparklet activity during AngII signaling. Interestingly, AKAP150 and TRPV4 channels dynamically interact along the cell's surface membrane. We propose that AKAP150 regulates local Ca^{2+} influx by targeting PKC to specific sarcolemmal domains where this kinase can modulate nearby TRPV4 channels.

The physiological implications of the opening of TRPV4 channels depend on the magnitude of the currents and Ca^{2+} signals they produce. Because TRPV4 channels are nonspecific cation channels, only a fraction of their total currents are carried by Ca^{2+} ions. We estimated the Ca^{2+} flux underlying elementary TRPV4 sparklets under physiological conditions (i.e., no EGTA in the cytosol) using the following equation:

$$J = \frac{\Delta\left[Ca^{2+}\right]_i \times B \times V}{T},$$

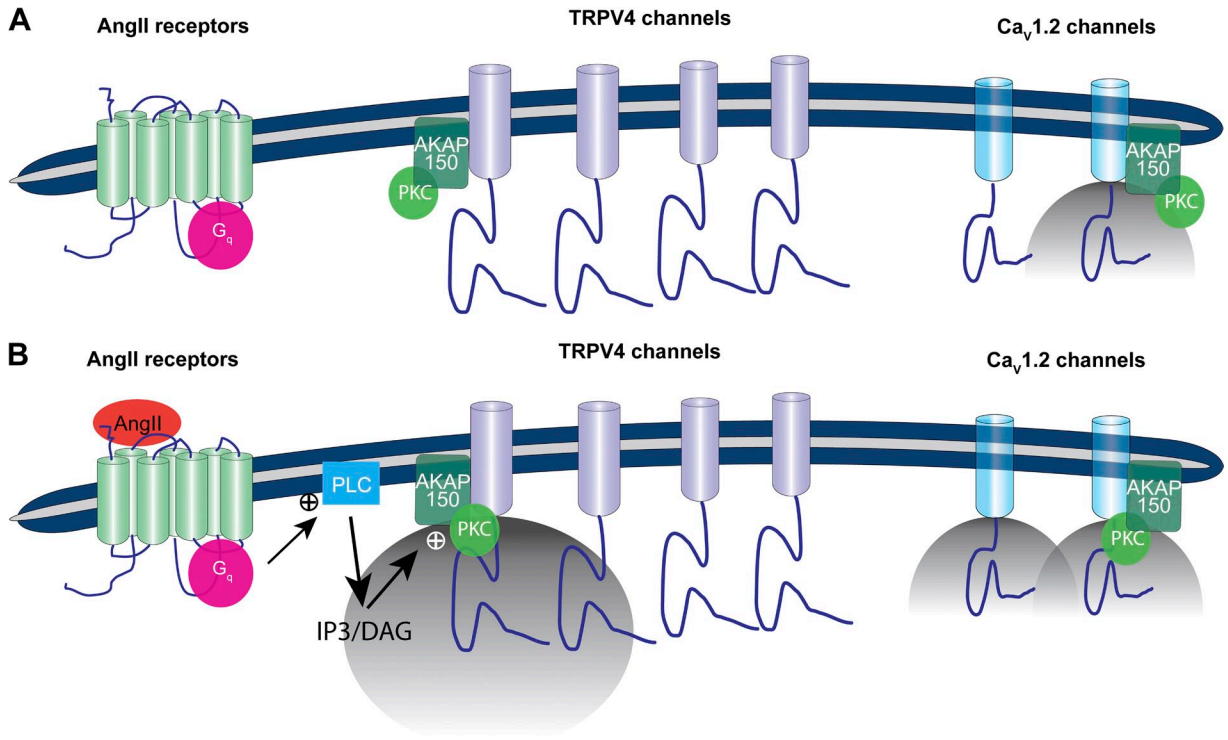

Figure 10. Proposed model for the local control of TRPV4 channels in arterial myocytes. (A) In this model, a subpopulation of $Ca_V1.2$ and TRPV4 channels is associated with AKAP150. This anchoring protein targets PKCα to the sarcolemma of arterial myocytes. Under basal conditions, TRPV4 sparklet activity is very low. Cytosolic Ca^{2+} is largely controlled by Ca^{2+} influx via voltage-gated $Ca_V1.2$ channels. (B) An increase in AngII levels activates G_q-coupled receptors, increasing cytosolic DAG and IP_3 levels. DAG activates AKAP150-anchored PKCα. Upon activation, PKCα can phosphorylate nearby TRPV4 and $Ca_V1.2$ channels, which increases the open probability of these channels. The opening of TRPV4 channels results in the production of large sparklets. Indeed, the total Ca^{2+} influx during a TRPV4 sparklets is ∼100-fold higher than during a $Ca_V1.2$ sparklet. However, the overall activity of $Ca_V1.2$ channels is much higher than that of TRPV4 channels. This limits TRPV4 sparklets to the regulation of local $[Ca^{2+}]_i$. A key feature of the proposed model is that AKAP150 and TRPV4 channels are mobile and could interact dynamically. Thus, the distance separating these proteins could change over time depending on physiological conditions. Accordingly, the location of TRPV4 sparklet activity could change over time depending on the proximity and activity of AKAP150-associated PKCα to these channels.

Downloaded from jgp.rupress.org on June 23, 2014

Published April 28, 2014

where J is the Ca^{2+} flux, $\Delta[Ca^{2+}]_i$ is the change in Ca^{2+} concentration, B is the Ca^{2+} buffering power of the cell, V is the volume occupied by the sparklet, and T is the open time of a TRPV4 channel. The calculation was performed using a T of 3 ms (Fecto et al., 2011), V of 10 fl, a volume similar to that occupied by a Ca^{2+} spark in the absence of EGTA (Cheng et al., 1993; Nelson et al., 1995), and B of 80 (Guerrero et al., 1994). With these conditions, a Ca^{2+} flux of 1.3×10^{-17} mol/s (equivalent to a current of ~2.5 pA) would produce a $\Delta[Ca^{2+}]_i$ of 50 nM. This estimate of Ca^{2+} flux implies that TRPV4 channels are highly permeable to Ca^{2+}, a conclusion that is compatible with our finding that TRPV4 sparklets are larger than $Ca_V1.2$ sparklets and two previous studies suggesting that TRPV4 channels are more permeable to Ca^{2+} than to Na^+ and K^+ (Liedtke et al., 2000; Strotmann et al., 2000).

The analysis described here also sheds light on why TRPV4 channels, but not $Ca_V1.2$ channels, can activate RyRs located in the junctional SR of arterial myocytes (Earley et al., 2005, 2009; Essin et al., 2007; Takeda et al., 2011). In principle, the coupling strength between RyRs and TRPV4 or $Ca_V1.2$ channels is determined by multiple factors including their proximity, the amplitude of the local $[Ca^{2+}]_i$ signal produced by sparklets, and the sensitivity of RyRs to Ca^{2+}. Although TRPV4 and $Ca_V1.2$ channels are expressed near the junctional SR, our data indicate that the total Ca^{2+} flux (i.e., signal mass) of a TRPV4 sparklet was nearly 100-fold higher than for a $Ca_V1.2$ sparklet. Thus, multiple $Ca_V1.2$ channels would have to open simultaneously to produce the same local Ca^{2+} signal as that of a single TRPV4 channel in an arterial myocyte. Although clusters of 2–6 $Ca_V1.2$ channels can open coordinately (Navedo et al., 2010), even these relatively rare coupled gating events would fall short of the Ca^{2+} flux through a single TRPV4 channel in arterial myocytes. The high flux of Ca^{2+} through individual TRPV4 channels allows for tight functional coupling between these channels and RyRs over a wider range of distances than for $Ca_V1.2$ channels in arterial myocytes.

It is important to note that although the Ca^{2+} flux associated with a TRPV4 sparklet is much higher than a $Ca_V1.2$ sparklet, the activity of TRPV4 sparklets is much lower than $Ca_V1.2$ sparklets, particularly over the physiological range of membrane potentials of arterial myocytes (−50 to −30 mV). This has an important functional consequence: it allows $Ca_V1.2$ sparklets to directly contribute to global increases in $[Ca^{2+}]_i$ and limits TRPV4 sparklets to the regulation of local $[Ca^{2+}]_i$. However, it is worth noting that given the large amplitude of TRPV4 sparklets, a large increase in the activity of these channels has the potential to increase both local and global $[Ca^{2+}]_i$ in cerebral arterial myocytes (Fig. 10).

Our study raises an important question: Why are a seemingly small number of these channels involved in Ca^{2+} influx in the cell? We propose a potential answer to this difficult question. Recent work from our laboratory demonstrated that AKAP150 targets PKC to the sarcolemma of arterial myocytes (Navedo et al., 2008). Furthermore, it was found that PKC expression was similar in WT and AKAP150$^{-/-}$ myocytes. In combination with the data presented here, these findings suggest that the low TRPV4 sparklet activity observed in AKAP150$^{-/-}$ myocytes was not caused by decreased levels of PKC, but rather by a lack of anchoring of this kinase to the sarcolemma, where it can modulate nearby TRPV4 channels during AngII signaling. Super-resolution localization maps revealed that AKAP150 and TRPV4 channels are expressed in puncta of varied sizes and proximities everywhere in the sarcolemma of these cells. In the model proposed here, the number and activity of TRPV4 sparklet sites is determined by the activities and spatial organization of G_q, DAG, AKAP150, PKC, and TRPV4 channels in arterial myocytes. Low TRPV4 sparklet activity could thus be caused by low local PKC activity or delocalization of this kinase. Because AKAP150 and TRPV4 channels are mobile and could interact dynamically, the distance separating these proteins could change over time depending on physiological conditions. Therefore, an interesting prediction of the model is that TRPV4 channel activity may not be restricted to a small, fixed number of channels. Instead, all TRPV4 channels in the membrane could potentially participate in Ca^{2+} influx. The specific subset of active TRPV4 channels could change with time depending on two factors: the proximity and activity of AKAP150-associated PKC to these channels. The opto-α1AR experiments showing that TRPV4-mediated Ca^{2+} influx could be induced wherever opto-α1AR and TRPV4 channels were expressed give credence to this view. Future experiments should test these predictions.

GSK-induced TRPV4 sparklets with similar amplitude and duration to those reported in this study have also been recorded from endothelial cells in mesenteric arteries (Sonkusare et al., 2012). These GSK-induced TRPV4 sparklets activate intermediate conductance, Ca^{2+}-sensitive K^+ channels, which hyperpolarize and relax connected arterial myocytes. Interestingly, the GSK-induced vasodilation reported in mesenteric arteries requires an intact endothelium. This suggests that mesenteric arterial myocytes do not express TRPV4 channels or that, if expressed, these channels are functionally silent. We found that GSK- and AngII-induced TRPV4 sparklet activity was significantly lower in AKAP150$^{-/-}$ myocytes. Thus, it is intriguing to speculate that regional variations in AKAP150 expression could contribute to differences in TRPV4 channel function throughout the vasculature. Regardless of the mechanisms underlying regional differences in TRPV4 channel activity or expression, these studies suggest that TRPV4 channels are key regulators of arterial function whether they are expressed in endothelial cells or myocytes.

Downloaded from jgp.rupress.org on June 23, 2014

Published April 28, 2014

To conclude, we propose that PKC, AKAP150, and TRPV4 channels form dynamic signaling domains that control Ca^{2+} influx in arterial myocytes. Activation of G_q-coupled AngII receptors enhances TRPV4 sparklet activity via activation of AKAP150-targeted PKC near these channels. In myocytes, TRPV4 sparklet activity seems to be regulated by the localization and activities of G_q-coupled receptors and AKAP150-targetd PKC. Together, these proteins form part of a dynamic feedback system that opposes vasoconstriction.

We thank Dr. Fred Rieke, Dr. Bertil Hille, Dr. Joshua Vaughan, Dr. Hill-Eubanks, and members of the Santana laboratory for reading the manuscript. Dr. R.E. Dixon helped with RICS and ccRICS analyses.

Support for this work was provided by Totman Medical Research Trust and grants P01HL095488, HL44455, HL098243, HL085870, GM048231, R37DK053832, HL098200, and COBRE (2-P20-RR-016435-06) from the National Institutes of Health.

The authors declare no competing financial interests.

Angus C. Nairn served as editor.

Submitted: 24 June 2013
Accepted: 2 April 2014

REFERENCES

Airan, R.D., K.R. Thompson, L.E. Fenno, H. Bernstein, and K. Deisseroth. 2009. Temporally precise in vivo control of intracellular signalling. *Nature.* 458:1025–1029. http://dx.doi.org/10.1038/nature07926

Amberg, G.C., and L.F. Santana. 2003. Downregulation of the BK channel β1 subunit in genetic hypertension. *Circ. Res.* 93:965–971. http://dx.doi.org/10.1161/01.RES.0000100068.43006.36

Amberg, G.C., M.F. Navedo, M. Nieves-Cintrón, J.D. Molkentin, and L.F. Santana. 2007. Calcium sparklets regulate local and global calcium in murine arterial smooth muscle. *J. Physiol.* 579:187–201. http://dx.doi.org/10.1113/jphysiol.2006.124420

Bayliss, W.M. 1902. On the local reactions of the arterial wall to changes of internal pressure. *J. Physiol.* 28:220–231.

Bolte, S., and F.P. Cordelières. 2006. A guided tour into subcellular colocalization analysis in light microscopy. *J. Microsc.* 224:213–232. http://dx.doi.org/10.1111/j.1365-2818.2006.01706.x

Cao, D.S., S.Q. Yu, and L.S. Premkumar. 2009. Modulation of transient receptor potential Vanilloid 4-mediated membrane currents and synaptic transmission by protein kinase C. *Mol. Pain.* 5:5. http://dx.doi.org/10.1186/1744-8069-5-5

Cheng, H., W.J. Lederer, and M.B. Cannell. 1993. Calcium sparks: elementary events underlying excitation-contraction coupling in heart muscle. *Science.* 262:740–744. http://dx.doi.org/10.1126/science.8235594

Digman, M.A., P.W. Wiseman, C. Choi, A.R. Horwitz, and E. Gratton. 2009a. Stoichiometry of molecular complexes at adhesions in living cells. *Proc. Natl. Acad. Sci. USA.* 106:2170–2175. http://dx.doi.org/10.1073/pnas.0806036106

Digman, M.A., P.W. Wiseman, A.R. Horwitz, and E. Gratton. 2009b. Detecting protein complexes in living cells from laser scanning confocal image sequences by the cross correlation raster image spectroscopy method. *Biophys. J.* 96:707–716. http://dx.doi.org/10.1016/j.bpj.2008.09.051

Dixon, R.E., C. Yuan, E.P. Cheng, M.F. Navedo, and L.F. Santana. 2012. Ca^{2+} signaling amplification by oligomerization of L-type $Ca_v1.2$ channels. *Proc. Natl. Acad. Sci. USA.* 109:1749–1754. http://dx.doi.org/10.1073/pnas.1116731109

Earley, S., B.J. Waldron, and J.E. Brayden. 2004. Critical role for transient receptor potential channel TRPM4 in myogenic constriction of cerebral arteries. *Circ. Res.* 95:922–929. http://dx.doi.org/10.1161/01.RES.0000147311.54833.03

Earley, S., T.J. Heppner, M.T. Nelson, and J.E. Brayden. 2005. TRPV4 forms a novel Ca^{2+} signaling complex with ryanodine receptors and BK_{Ca} channels. *Circ. Res.* 97:1270–1279. http://dx.doi.org/10.1161/01.RES.0000194321.60300.d6

Earley, S., T. Pauyo, R. Drapp, M.J. Tavares, W. Liedtke, and J.E. Brayden. 2009. TRPV4-dependent dilation of peripheral resistance arteries influences arterial pressure. *Am. J. Physiol. Heart Circ. Physiol.* 297:H1096–H1102. http://dx.doi.org/10.1152/ajpheart.00241.2009

Essin, K., A. Welling, F. Hofmann, F.C. Luft, M. Gollasch, and S. Moosmang. 2007. Indirect coupling between $Ca_v1.2$ channels and ryanodine receptors to generate Ca^{2+} sparks in murine arterial smooth muscle cells. *J. Physiol.* 584:205–219. http://dx.doi.org/10.1113/jphysiol.2007.138982

Fan, H.C., X. Zhang, and P.A. McNaughton. 2009. Activation of the TRPV4 ion channel is enhanced by phosphorylation. *J. Biol. Chem.* 284:27884–27891. http://dx.doi.org/10.1074/jbc.M109.028803

Fecto, F., Y. Shi, R. Huda, M. Martina, T. Siddique, and H.X. Deng. 2011. Mutant TRPV4-mediated toxicity is linked to increased constitutive function in axonal neuropathies. *J. Biol. Chem.* 286:17281–17291. http://dx.doi.org/10.1074/jbc.M111.237685

Fleischmann, B.K., R.K. Murray, and M.I. Kotlikoff. 1994. Voltage window for sustained elevation of cytosolic calcium in smooth muscle cells. *Proc. Natl. Acad. Sci. USA.* 91:11914–11918. http://dx.doi.org/10.1073/pnas.91.25.11914

Fölling, J., M. Bossi, H. Bock, R. Medda, C.A. Wurm, B. Hein, S. Jakobs, C. Eggeling, and S.W. Hell. 2008. Fluorescence nanoscopy by ground-state depletion and single-molecule return. *Nat. Methods.* 5:943–945. http://dx.doi.org/10.1038/nmeth.1257

Guerrero, A., J.J. Singer, and F.S. Fay. 1994. Simultaneous measurement of Ca^{2+} release and influx into smooth muscle cells in response to caffeine. A novel approach for calculating the fraction of current carried by calcium. *J. Gen. Physiol.* 104:395–422. http://dx.doi.org/10.1085/jgp.104.2.395

Harder, D.R., R. Gilbert, and J.H. Lombard. 1987. Vascular muscle cell depolarization and activation in renal arteries on elevation of transmural pressure. *Am. J. Physiol.* 253:F778–F781.

Heisenberg, W. 1930. The Physical Principles of Quantum Theory. The University of Chicago Press, Chicago. 208 pp.

Hoshi, N., L.K. Langeberg, C.M. Gould, A.C. Newton, and J.D. Scott. 2010. Interaction with AKAP79 modifies the cellular pharmacology of PKC. *Mol. Cell.* 37:541–550. http://dx.doi.org/10.1016/j.molcel.2010.01.014

Idevall-Hagren, O., E.J. Dickson, B. Hille, D.K. Toomre, and P. De Camilli. 2012. Optogenetic control of phosphoinositide metabolism. *Proc. Natl. Acad. Sci. USA.* 109:E2316–E2323. http://dx.doi.org/10.1073/pnas.1211305109

Jaggar, J.H., G.C. Wellman, T.J. Heppner, V.A. Porter, G.J. Perez, M. Gollasch, T. Kleppisch, M. Rubart, A.S. Stevenson, W.J. Lederer, et al. 1998. Ca^{2+} channels, ryanodine receptors and $Ca^{(2+)}$-activated K^+ channels: a functional unit for regulating arterial tone. *Acta Physiol. Scand.* 164:577–587. http://dx.doi.org/10.1046/j.1365-201X.1998.00462.x

Lachmanovich, E., D.E. Shvartsman, Y. Malka, C. Botvin, Y.I. Henis, and A.M. Weiss. 2003. Co-localization analysis of complex formation among membrane proteins by computerized fluorescence microscopy: application to immunofluorescence copatching studies. *J. Microsc.* 212:122–131. http://dx.doi.org/10.1046/j.1365-2818.2003.01239.x

Liedtke, W., Y. Choe, M.A. Martí-Renom, A.M. Bell, C.S. Denis, A. Sali, A.J. Hudspeth, J.M. Friedman, and S. Heller. 2000. Vanilloid

Downloaded from jgp.rupress.org on June 23, 2014

Published April 28, 2014

receptor-related osmotically activated channel (VR-OAC), a candidate vertebrate osmoreceptor. *Cell.* 103:525–535. http://dx.doi.org/10.1016/S0092-8674(00)00143-4

Narayanan, D., S. Bulley, M.D. Leo, S.K. Burris, K.S. Gabrick, F.A. Boop, and J.H. Jaggar. 2013. Smooth muscle cell transient receptor potential polycystin-2 (TRPP2) channels contribute to the myogenic response in cerebral arteries. *J. Physiol.* 591:5031–5046. http://dx.doi.org/10.1113/jphysiol.2013.258319

Navedo, M.F., G.C. Amberg, V.S. Votaw, and L.F. Santana. 2005. Constitutively active L-type Ca^{2+} channels. *Proc. Natl. Acad. Sci. USA.* 102:11112–11117. http://dx.doi.org/10.1073/pnas.0500360102

Navedo, M.F., G.C. Amberg, M. Nieves, J.D. Molkentin, and L.F. Santana. 2006. Mechanisms underlying heterogeneous Ca^{2+} sparklet activity in arterial smooth muscle. *J. Gen. Physiol.* 127:611–622. http://dx.doi.org/10.1085/jgp.200609519

Navedo, M.F., M. Nieves-Cintrón, G.C. Amberg, C. Yuan, V.S. Votaw, W.J. Lederer, G.S. McKnight, and L.F. Santana. 2008. AKAP150 is required for stuttering persistent Ca^{2+} sparklets and angiotensin II-induced hypertension. *Circ. Res.* 102:e1–e11. http://dx.doi.org/10.1161/CIRCRESAHA.107.167809

Navedo, M.F., E.P. Cheng, C. Yuan, S. Votaw, J.D. Molkentin, J.D. Scott, and L.F. Santana. 2010. Increased coupled gating of L-type Ca^{2+} channels during hypertension and Timothy syndrome. *Circ. Res.* 106:748–756. http://dx.doi.org/10.1161/CIRCRESAHA.109.213363

Nelson, M.T., H. Cheng, M. Rubart, L.F. Santana, A.D. Bonev, H.J. Knot, and W.J. Lederer. 1995. Relaxation of arterial smooth muscle by calcium sparks. *Science.* 270:633–637. http://dx.doi.org/10.1126/science.270.5236.633

Rossow, M.J., J.M. Sasaki, M.A. Digman, and E. Gratton. 2010. Raster image correlation spectroscopy in live cells. *Nat. Protoc.* 5:1761–1774. http://dx.doi.org/10.1038/nprot.2010.122

Rubart, M., J.B. Patlak, and M.T. Nelson. 1996. Ca^{2+} currents in cerebral artery smooth muscle cells of rat at physiological Ca^{2+} concentrations. *J. Gen. Physiol.* 107:459–472. http://dx.doi.org/10.1085/jgp.107.4.459

Schermelleh, L., R. Heintzmann, and H. Leonhardt. 2010. A guide to super-resolution fluorescence microscopy. *J. Cell Biol.* 190:165–175. http://dx.doi.org/10.1083/jcb.201002018

Sonkusare, S.K., A.D. Bonev, J. Ledoux, W. Liedtke, M.I. Kotlikoff, T.J. Heppner, D.C. Hill-Eubanks, and M.T. Nelson. 2012. Elementary Ca^{2+} signals through endothelial TRPV4 channels regulate vascular function. *Science.* 336:597–601. http://dx.doi.org/10.1126/science.1216283

Spassova, M.A., T. Hewavitharana, W. Xu, J. Soboloff, and D.L. Gill. 2006. A common mechanism underlies stretch activation and receptor activation of TRPC6 channels. *Proc. Natl. Acad. Sci. USA.* 103:16586–16591. http://dx.doi.org/10.1073/pnas.0606894103

Strotmann, R., C. Harteneck, K. Nunnenmacher, G. Schultz, and T.D. Plant. 2000. OTRPC4, a nonselective cation channel that confers sensitivity to extracellular osmolarity. *Nat. Cell Biol.* 2:695–702. http://dx.doi.org/10.1038/35036318

Takeda, Y., M.A. Nystoriak, M. Nieves-Cintrón, L.F. Santana, and M.F. Navedo. 2011. Relationship between Ca^{2+} sparklets and sarcoplasmic reticulum Ca^{2+} load and release in rat cerebral arterial smooth muscle. *Am. J. Physiol. Heart Circ. Physiol.* 301:H2285–H2294. http://dx.doi.org/10.1152/ajpheart.00488.2011

Thorneloe, K.S., A.C. Sulpizio, Z. Lin, D.J. Figueroa, A.K. Clouse, G.P. McCafferty, T.P. Chendrimada, E.S. Lashinger, E. Gordon, L. Evans, et al. 2008. *N*-((1*S*)-1-{[4-((2*S*)-2-{[(2,4-Dichlorophenyl)sulfonyl]amino}-3-hydroxypropanoyl)-1-piperazinyl]carbonyl}-3-methylbutyl)-1-benzothiophene-2-carboxamide (GSK1016790A), a Novel and Potent Transient Receptor Potential Vanilloid 4 Channel Agonist Induces Urinary Bladder Contraction and Hyperactivity: Part I. *J. Pharmacol. Exp. Ther.* 326:432–442. http://dx.doi.org/10.1124/jpet.108.139295

Watanabe, H., J. Vriens, J. Prenen, G. Droogmans, T. Voets, and B. Nilius. 2003. Anandamide and arachidonic acid use epoxyeicosatrienoic acids to activate TRPV4 channels. *Nature.* 424:434–438. http://dx.doi.org/10.1038/nature01807

Welsh, D.G., A.D. Morielli, M.T. Nelson, and J.E. Brayden. 2002. Transient receptor potential channels regulate myogenic tone of resistance arteries. *Circ. Res.* 90:248–250. http://dx.doi.org/10.1161/hh0302.105662

Zenisek, D., V. Davila, L. Wan, and W. Almers. 2003. Imaging calcium entry sites and ribbon structures in two presynaptic cells. *J. Neurosci.* 23:2538–2548.

Zhang, X., L. Li, and P.A. McNaughton. 2008. Proinflammatory mediators modulate the heat-activated ion channel TRPV1 via the scaffolding protein AKAP79/150. *Neuron.* 59:450–461. http://dx.doi.org/10.1016/j.neuron.2008.05.015

ZhuGe, R., K.E. Fogarty, R.A. Tuft, L.M. Lifshitz, K. Sayar, and J.V. Walsh Jr. 2000. Dynamics of signaling between Ca^{2+} sparks and Ca^{2+}-activated K^+ channels studied with a novel image-based method for direct intracellular measurement of ryanodine receptor Ca^{2+} current. *J. Gen. Physiol.* 116:845–864. http://dx.doi.org/10.1085/jgp.116.6.845

Zou, H., L.M. Lifshitz, R.A. Tuft, K.E. Fogarty, and J.J. Singer. 2002. Visualization of Ca^{2+} entry through single stretch-activated cation channels. *Proc. Natl. Acad. Sci. USA.* 99:6404–6409. http://dx.doi.org/10.1073/pnas.092654999

Downloaded from jgp.rupress.org on June 23, 2014

Mercado et al., http://www.jgp.org/cgi/content/full/jgp.201311050/DC1

THE JOURNAL OF GENERAL PHYSIOLOGY

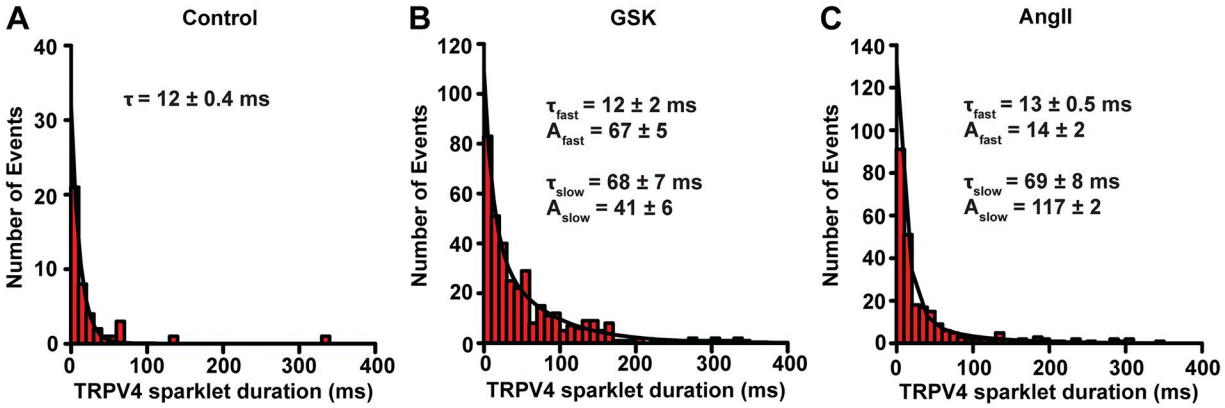

Figure S1. GSK and AngII increase the duration of TRPV4 sparklet in arterial myocytes. Histograms of the duration of TRPV4 sparklet sites in arterial myocytes under control conditions (A) and after application of 100 nM GSK (B) or 100 nM AngII (C). The black line in A is a fit to the data with a single exponential function $y = Ae^{(-x/\tau)} + y_i$, where A is the amplitude, τ is the time constant, and y_i is the y intercept. The black lines in C and D are fits with a double exponential function $y = A_{fast}e^{(-x/\tau_{fast})} + A_{slow}e^{(-x/t_{slow})} + y_i$, where A_{fast} and A_{slow} are the amplitudes of the fast and slow component, respectively, and τ_{fast} and τ_{slow} are the fast and slow time constants, respectively.

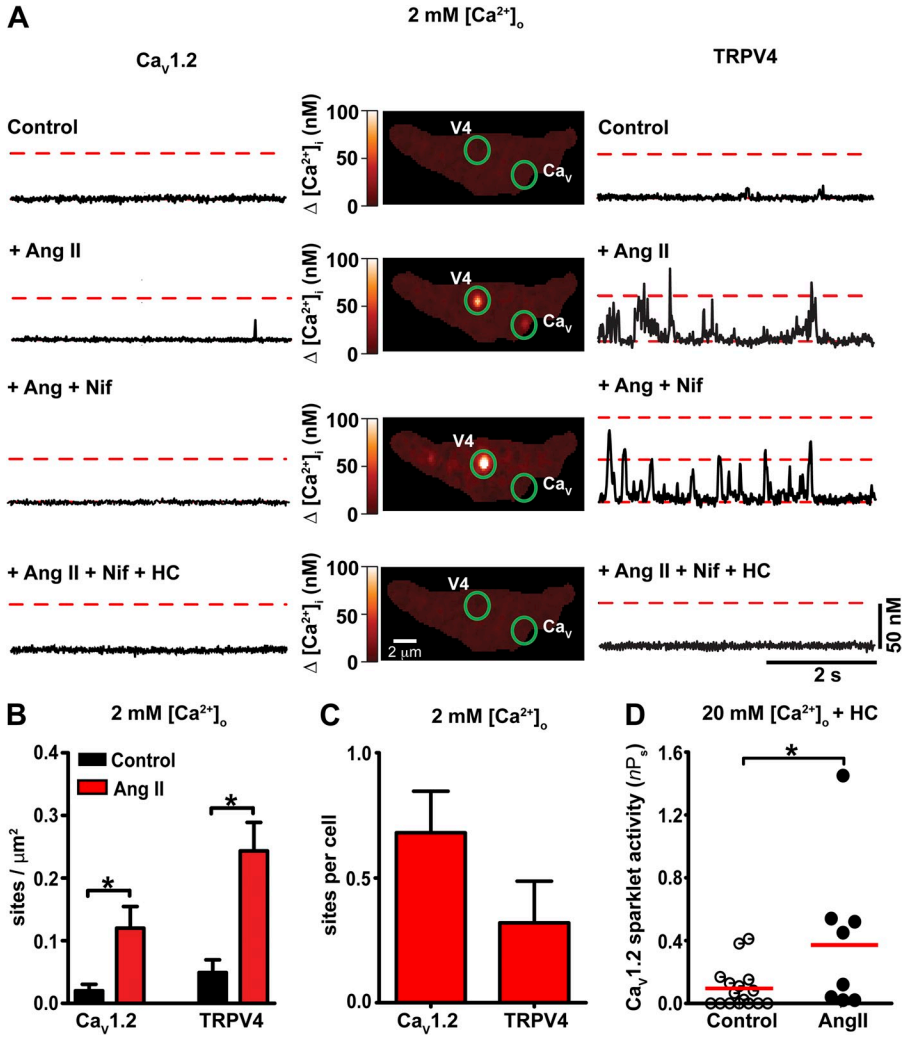

Figure S2. AngII increased $Ca_v1.2$ and TRPV4 sparklet activities in arterial myocytes. (A) $Ca_v1.2$ (left) and TRPV4 (right) sparklet records from a representative myocytes before (control) and after application of 100 nM AngII, AngII + 1 μM nifedipine, and AngII, Nif, and HC-067047 (1 μM). Traces are from the regions of the cell with $Ca_v1.2$ (Ca_v) and TRPV4 (V4) sparklets. The experiments in this panel were performed in the presence of 2 mM external Ca^{2+}. (B) Bar plot of the density of $Ca_v1.2$ ($n = 7$) and TRPV4 ($n = 5$) sparklet before and after application of AngII in the presence of 2 mM $[Ca^{2+}]_o$. Data are means ± SEM (error bars; *, $P < 0.05$; one-tailed Student's *t* test). (C) Mean number ± SEM (error bars) of $Ca_v1.2$ and TRPV4 sparklet events per cell after application of AngII ($n = 3$). (D) $Ca_v1.2$ sparklet activity before and after application of AngII in the continuous presence of 1 μM HC-067047, but in 20 mM $[Ca^{2+}]_o$. The red lines are the median values (*, $P < 0.05$, $n = 16$; Mann-Whitney test).

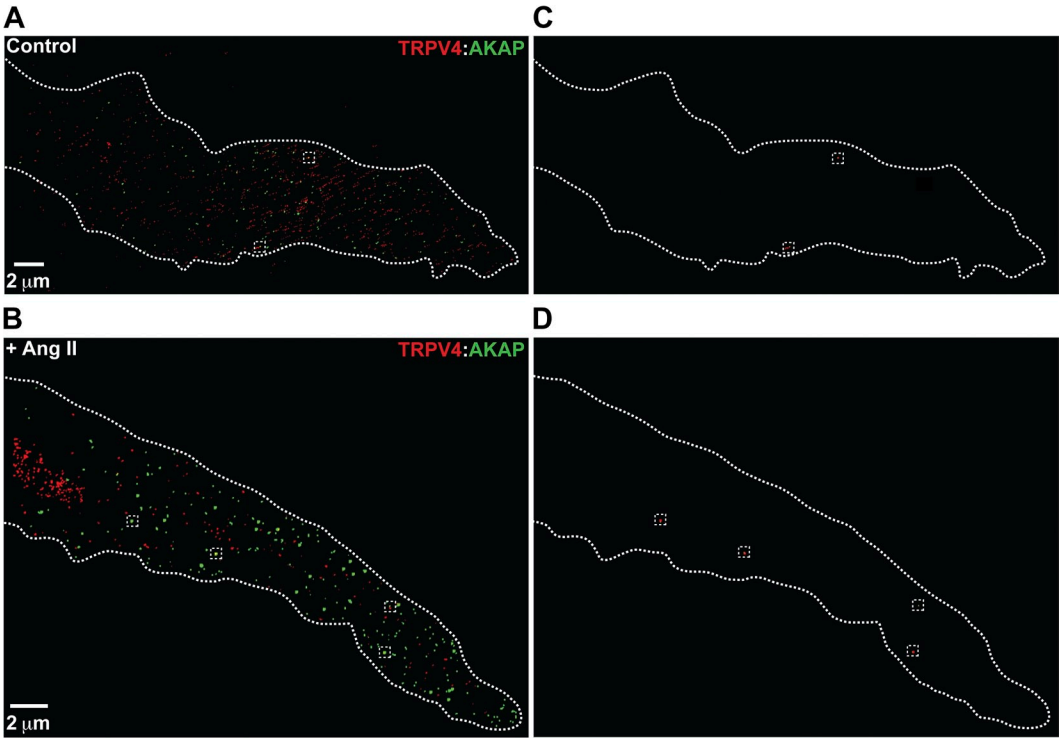

Figure S3. AKAP150 and TRPV4 colocalization increased upon AngII exposure. Super-resolution localization maps of AKAP150 and TRPV4 from a control cell (A) and a cell exposed to 100 nM AngII (B) before fixation. The images in C and D show the puncta in the control (A) and AngII-treated (B) cell where TRPV4 and AKAP150 overlapped (boxed regions). The broken lines indicate the outlines of the cells.